

# Numerical Electromagnetic Analysis of Lightning Surge Response on Vertical Conductor

by

**Md. Salah Uddin Yusuf**



A thesis

Submitted to the Department of Electrical & Electronic Engineering, Khulna University of Engineering & Technology (KUET) in partial fulfillment of the requirements for the degree

of

**Master of Science**

in

Electrical & Electronic Engineering



Faculty of Electrical & Electronic Engineering  
Khulna University of Engineering & Technology (KUET)  
Khulna-920300  
May 16, 2005

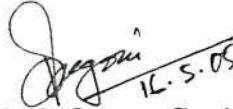
This Dissertation Entitled  
**"Numerical Electromagnetic Analysis of Lightning Surge  
Response on Vertical Conductor"**

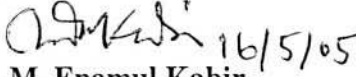
by

**Md. Salah Uddin Yusuf**

Submitted to the Department of Electrical & Electronic Engineering, Khulna University of Engineering & Technology (KUET), in partial fulfillment of the requirements for Degree of **Master of Science** in Electrical & Electronic Engineering is hereby accepted.

**Dissertation Committee**

  
**Dr. Md. Osman Goni** (Supervisor) Chairman  
Assistant Professor  
Department of Electronics & Communication Engg.  
Khulna University of Engineering & Technology, Khulna.

  
**Mr. A. N. M. Enamul Kabir** Member  
Associate Professor & Head of the Department  
Department of Electrical & Electronic Engg.  
Khulna University of Engineering & Technology, Khulna.

  
**Professor Dr. Abdur Rahim Mollah** Member  
Department of Electrical & Electronic Engg.  
Khulna University of Engineering & Technology, Khulna.

  
**Dr. Md. Rafiqul Islam** Member  
Assistant Professor  
Department of Electrical & Electronic Engg.  
Khulna University of Engineering & Technology, Khulna.

  
**Professor Dr. Md. Ruhul Amin** Member (External)  
Department of Electrical & Electronic Engg.  
Rajshahi University of Engineering & Technology, Rajshahi.

**Khulna University of Engineering & Technology (KUET), Khulna.  
Khulna-920300, Bangladesh.  
May, 2005.**

## Acknowledgements

At first, the author would like to prostrate in worship to Almighty Allah, Who give him mercy and power to complete his M.Sc. Engineering program successfully.

The author would like to express his deepest gratitude to Dr. Md. Osman Goni, Assistant Professor, Dept. of Electronics & Communication Engineering, Faculty of Electrical & Electronic Engineering for supervising and encouraging him to complete this thesis successfully. He gave the author opportunities to participate in the research conferences in which the author was able to know about the current research in this regard which inspired the author very much. Without his continuous proper guidance it was impossible to complete this research.

The author wishes to express his sincere appreciation to Prof. Dr. Md. Abul Kalam Azad, Head of the Dept. of Computer Science & Engineering for his encouragement, precious comment and valuable suggestion, which encouraged him all the time.

The author is very much grateful to the members of the committee for their involvement in providing direction for this dissertation and reviewing the work.

The author would like to thank all the members of the faculty of Electrical & Electronic Engineering of the University for their encouragement at different times.

Finally, the author wishes to thank his family, relatives and colleagues, for their great support and continuous encouragement through their love and prayers to complete the study and research.

**AUTHOR**

May 2005



## Abstract

In analyzing the lightning performance of overhead power transmission lines and substations, the lightning surge characteristics of transmission line components as well as the statistical data of lightning such as the ground flash density and the stroke peak current distributions are essential. Among the transmission line components, tower surge characteristics including the tower footing impedance characteristics in the linear region are probably the most fundamental factors since they contribute directly to the insulator voltages during a lightning hit. Particularly for such tall structure as EHV or UHV double-circuit towers, the characteristics become more dominant owing to the longer round-trip time of a travelling wave in the tower. An agreement on the interpretation of this phenomenon, however, has not been reached yet.

There have been three considerations to evaluate the transient characteristics of a tower as follows: (i) theoretical studies, (ii) simulation of reduced scale models and (iii) simulation of full-sized tower. Measurement on full-sized towers is straightforward in evaluating the actual characteristics of a tower struck by lightning, however it is difficult to carry out this kind of experiments in the ideal arrangement where a current lead wire is stretched vertically above the tower top to simulate a lightning channel, owing to its scale. Measurement on reduced scale models is more economical than full-sized towers, and is flexible in setting up various experimental arrangements. It is however not easy to maintain the accuracy. Theoretical studies on simplified geometry may be useful in understanding the phenomenon, however, they are invalid for the accurate evaluation of the dynamic electromagnetic behavior of a three dimensional (3-D) system struck by lightning.

The simulation analysis of surge response are carried out in the several arrangements of the current lead wire: (i) vertical and at the top of vertical conductor, (ii) vertical and a little far from the top of vertical conductor, and (iii) horizontal and far from the top of vertical conductor. In all the cases, the voltage measuring wire is placed at the perpendicular to the current lead wire. Each of the arrangement of the current lead wire affects the measured surge impedance of the vertical conductor and that has been explained in this research in detail. If a travelling wave propagates along the vertical conductor at the velocity of light, the reflected wave from the ground should return to the



top of the vertical conductor just after the round-trip time of the travelling wave in the vertical conductor.

For the accurate analysis of the dynamic electromagnetic field around a complex tower system struck by lightning, electromagnetic modeling codes are appropriate. Of many available codes, the Numerical Electromagnetic Code (NEC-2) based on the Method of Moments is chosen for the present work, since it has been widely and successfully used in analyzing thin-wire antennas and a tower system can be regarded as a thin-wire antenna.

In the present thesis, firstly, the applicability of NEC-2 to the electromagnetic field analysis of vertical conductor surge response is verified by comparison with theoretical results on simple structure.

Secondly, four parallel conductors model are taken into account for the analysis by NEC-2 to evaluate the surge characteristics. Thirdly, the surge characteristics of actual tower struck by lightning are studied with the help of NEC-2.

Finally, it can be concluded that this research presents some results concerning the simulation of electromagnetic transient in transmission lines caused by direct and indirect strikes of lightning, which will help to design the structure of tower and to design lightning arrester to protect various electric appliances that is used in our everyday life.

# Contents

<b>1. Introduction</b>	<b>3</b>
1.1 Lightning	3
1.1.1 Lightning Formation	3
1.1.2 The Most Common Types of Lightning	4
1.1.3 Approximate Lightning Parameters	4
1.1.4 Lightning Effects on Power Systems	5
1.2 History of Lightning Surge Analysis	7
1.3 Electromagnetic Simulation Technique	9
1.4 Electromagnetic Modeling Code	11
1.5 Objective and Scope of the Thesis	12
<b>2. Application of NEC-2 Code to the Analysis of Surge Response</b>	<b>13</b>
2.1 Introduction	13
2.2 Electric Field Integral Equation	13
2.3 Numerical Solution by the Method of Moments	16
2.4 Structure Modeling Guideline	20
2.5 Example of Input Data to NEC-2	23
2.6 Theoretical Formula of Surge Impedances	25
2.7 Application to Analysis of Vertical Conductor Surge Response	26
2.8 Surge Simulation by NEC-2	30
2.8.1 With Ground Plane	30
2.8.2 Without Ground Plane	30
2.8.3 Surge Impedances	33
2.8.4 Influence of the Method of Current Injection	37
2.8.5 Effect of Changing Segment Length	38
2.8.6 Effect of Changing Radius and Height	39
2.8.7 Computation Time	40
2.9 Summary	40
<b>3. Surge Analysis of Four Parallel Conductors</b>	<b>42</b>
3.1 Introduction	42
3.2 With Ground Plane	43
3.3 Without Ground Plane	45
3.4 Surge Impedances	47
3.5 Computation Time	47
3.6 Summary	48
<b>4. Surge Analysis of Actual Tower Model</b>	<b>49</b>
4.1 Introduction	49
4.2 Numerical Electromagnetic Analysis of Earth-Wired Tower Struck by Lightning	49
4.3 With Ground Plane	53
4.4 Without Ground Plane	53

4.5 Surge Impedances	54
4.6 Influence of the Arrangement of Current Lead Wire	55
4.7 Estimation of Surge Impedance of Double-Circuit Transmission Tower	56
4.8 Computation Time	58
4.8 Summary	58
<b>5. Conclusions</b>	<b>59</b>
<b>Bibliography</b>	<b>61</b>
<b>Appendix</b>	<b>64</b>
A History and Availability of NEC-MoM Codes	64
B Sample Input Data to NEC-2 for Single Vertical Conductor Model	67
C Sample Input Data to NEC-2 for Four Parallel Vertical Conductors Model	70
D Sample Input Data to NEC-2 for Actual Tower Model	75





# Chapter 1

## Introduction

### 1.1 Lightning

Lightning is an electrical discharge in the atmosphere, representing a rapid flow of electrical charge between

- (i) a cloud and the ground - CG (Cloud to Ground),
- (ii) between two clouds - CC (Cloud to Cloud) or inter cloud lightning,
- (iii) between two portions of the same cloud - CC (Cloud to Cloud) or intra cloud lightning.

#### 1.1.1 Lightning Formation

(i) The conditions needed to produce lightning have been known for some time. However, exactly how lightning forms have never been verified. Leading theories focus around separation of electric charge and generation of an electric field within a thunderstorm. Recent studies also indicate that ice, hail, and semi-frozen water drops known as graupel are essential to lightning development. Storms that fail to produce large quantities of ice usually fail to produce lightning.

(ii) Thunderstorms have very turbulent environments. Strong updrafts and downdrafts occur with regularity and within close proximity to each other. The updrafts transport small liquid water droplets from the lower regions of the storm to heights between 35,000 and 70,000 feet above the freezing level. Meanwhile, downdrafts transport hails and ice from the frozen upper regions of the storm. When these collide, the water droplets freeze and release heat. This heat in turn keeps the surface of the hail and ice slightly warmer than its surrounding environment, and a “soft hail”, or “graupel” forms. As the ice particles within a cloud (called hydrometers) grow and interact, they collide, fracture and break apart. It is thought that the smaller particles tend to acquire positive charge, while the larger particles acquire more negative charge. These particles tend to separate under the influences of updrafts and gravity until the upper portion of the cloud acquires a net positive charge and the lower portion of the cloud becomes negatively charged. This separation of charge produces enormous electrical potential both within the cloud and between the cloud and ground. This

can accumulate to millions of volts, and eventually the electrical resistance in the air breaks down and a flash begins.

### 1.1.2 The Most Common Types of Lightning

(i) Cloud-to-ground lightning is the most damaging and dangerous form of lightning. Although not the most common type, it is the one, which is best understood. Most flashes originate near the lower negative charge center and deliver negative charge to earth. However, appreciable minorities of flashes carry positive charge to earth. These positive flashes often occur during the dissipating stage of a thunderstorm's life. Positive flashes are also more common as a percentage of total ground strikes during the winter months.

(ii) Intra-cloud lightning is the most common type of discharge. This occurs between oppositely charged centers within the same cloud. Usually the process takes place within the cloud and looks from the outside of the cloud like a diffuse brightening which flickers. However, the flash may exit the boundary of the cloud and a bright channel, similar to a cloud-to-ground flash, can be visible for many miles.

(iii) Inter-cloud lightning, as the name implies, occurs between charge centers in two different clouds with the discharge bridging a gap of clear air between them.

These various types of lightning causes fire in the forest, voltage surge in the power lines, high electric field and arching inside the building, explosions for industrial sites housing volatile compounds and military sites housing explosives and malfunctioning in telecommunication system or not functioning at all.

### 1.1.3 Approximate Lightning Parameter [1]

Voltage (relative to ground)	1.0E+8 to 1.0E+9 V
Current	100 A
Peak current	30,000 A
Duration	0.001 - 0.5 s
Diameter of the current channel	0.1 m
Diameter of the luminous region	1-10 m
Typical length	5.0E3 m
Plasma Temperature	to 3 eV
Electron density	1.0E+23 to 1.0E+24 electrons/cubic meter
% power into visible light	1-3
% power into sound	10-50
% power into heat	10-50
% power into radio waves	10-50
Peak magnetic field created	1000 G



#### 1.1.4 Lightning Effects on Power Systems

The frequency of thunderstorms is important in the protection of power systems. The frequency of occurrence of strokes to transmission lines and open circuit is an indication of the exposure to lightning that an electric power system experiences.

In designing lightning protection for power systems, how lightning enters the system, both by direct strokes and by induced surges from nearby strokes; the propagation of surges within the system and the effects of these surge voltages and currents on the circuits and apparatus within the system must be considered as follows:

(i) Lightning surges entering a power system through direct strokes are the primary concern in planning surge protection. These strokes may hit phase conductors directly, or they may strike the overhead ground wires or masts that shield the conductors. So, it is necessary to understand the associated surge currents and voltages produced before a protection system can be designed.

(ii) A lightning stroke terminating directly on phase conductors or equipment terminals develops a very high voltage, which, with no surge protection, will flash over the insulation in the majority of cases. If the flashover occurs through air or across porcelain insulation, it rarely causes permanent damage.

a. A lightning stroke terminating near a transmission line can induce a voltage in the circuit, which seldom exceeds 500 kV. Lines, shielded with overhead ground wires and operating at 69 kV and above, generally have sufficient insulation to prevent flashover by voltages in this range. Lower voltage lines, however, with insulation levels appreciably below 500 kV, may be flashed over by induced surges.

b. A lightning stroke terminating on a power system initiates traveling waves, which propagate within the system. To determine the resulting surge voltages and currents in various parts of the system, a traveling wave analysis is required. Simple networks with linear impedances can be analyzed manually; more complicated networks, characteristic of practical power systems, require analog or digital computer analysis. First, consider a stroke terminating on the phase conductor of a transmission line. The stroke initiates voltage and current waves traveling at the speed of light in each direction from the terminating point. With linear impedance, voltage and current have the same waveshape. The traveling waves are represented by the equation:  $e = iZ$ , where  $e$  and  $i$  are the voltage and current of the traveling wave and  $Z$  is the conductor surge impedance respectively.

(iii) Surge impedance is circuit impedance as seen by a transient such as lightning. For an open wire conductor:



$$Z = L/C$$

$L$  = inductance/unit length

$C$  = shunt capacitance to ground/unit length

(iv) Typical surge impedance for a line conductor is 400  $\Omega$ . Corresponding values for  $L$  and  $C$  would be 0.4 H/feet and 2.5 pF/feet, respectively.

(v) Assuming that the stroke current,  $I$ , is equal to  $2i$  (that is, the stroke current divides equally at the terminating point), the conductor voltage for a 10,000 A stroke is:

$$\begin{aligned} e &= IZ / 2 = \frac{10000}{2} \times 400 \text{ kV} \\ &= 2000 \text{ kV} \end{aligned}$$

Thus, a traveling wave current of 5,000 A ( $I/2$ ) generates 2,000 kV on the transmission line.

(vi) The traveling waves initiated by the stroke continue to propagate along the line until a discontinuity is encountered. At this point, voltage and current waves are reflected back along the line, and at the same time, traveling waves are transmitted beyond the point of discontinuity. Points of discontinuity may be an open circuit breaker, a transformer, another connected line, or a flashover on the line.

To a lightning surge, a transformer appears as a capacitance and behaves essentially as an open circuit. As the traveling voltage wave encounters an open circuit, a voltage wave of the same magnitude and polarity as the incoming surge is reflected. The incoming and reflected waves combine, resulting in double the traveling wave voltage ( $2e$ ) at the open circuit or transformer termination. This is the well-known phenomenon of voltage doubling at the end of a line.

(a) For an open circuit termination, the reflected current wave has the same magnitude as, but opposite polarity to the incoming waves, resulting in zero current at the open end of a line.

(b) Now consider a line terminated in a perfect short circuit. The incoming and reflected voltage waves have the same magnitude and opposite polarity resulting in zero voltage at the terminal. The current waves have equal magnitude and the same polarity, resulting in double the traveling wave current ( $2I$ ). This is the well-known phenomenon of traveling wave current doubling when it encounters a short circuit.

(c) An arrester discharging a current at the end of a line is a close approximation to the short circuit case, since the arrester resistance is very low compared with the line surge impedance. The current, which the arrester must discharge, therefore, is nearly double the

line traveling wave current. This is an important concept in considering arrester discharge duty from lightning surges.

(d) This simple calculation illustrates the advantages of multiple lines in reducing surge voltage in a substation.

(e) As noted previously, typical surge impedance for a phase conductor is  $400 \Omega$ . Some other typical values are:

Overhead ground wire –  $450$  to  $500 \Omega$

Two overheads ground wires (in parallel) –  $350 \Omega$

Steel transmission tower –  $200 \Omega$

Cables –  $15$  to  $40 \Omega$

(f) The propagation velocity in each of these elements is essentially that of light, with the exception of cables in which propagation velocity is about 50 % of that of light, depending on the dielectric constant of the insulating material. These values are useful in representing power systems in detailed traveling wave analysis using analog or digital computer methods.

(vii) In protecting power systems against lightning, surge voltages and currents must be considered. A lightning stroke to a power system develops very high surge voltages across equipment and line insulation systems. If these voltages exceed the insulation strength, a flashover occurs. A flashover through air or over porcelain insulation (commonly used for transmission line insulation) does not usually produce permanent damage.

(vii) Once lightning enters a power system, the surge current is unlikely to cause any damage. Although the current may be extremely high, it is very short lived and can easily be handled by a small conductor. The size of conductors, installed expressly for conducting lightning currents, is usually determined by mechanical strength considerations, rather than by current-carrying capacity. This is probably due to the stroke channel heating the conductor at the point of impingement, rather than from simply conducting the lightning current.

## 1.2 History of Lightning Surge Impedance

For overhead transmission lines, lightning is the primary cause of unscheduled interruption. Prediction of lightning surges is very important for the design of electric power systems and telecommunication systems. In particular, tower surge impedance is an important factor in analysis of the lightning performance of transmission lines. Therefore, a number of theoretical studies and experimental on tower surge impedance have been carried

out [2]-[11] different times. The formula given by various researcher are given below:

- (i) 1934 - Jordan's equation by Jordan of GE

$$Z = 60 \left\{ \ln \left( \frac{2\sqrt{2}h}{r} \right) - 2.0397 \right\}$$

- (ii) 1956 - Theoretical Formula due to Electromagnetic Field theory by C.F. Wagner

- (iii) 1957 - The Theoretical Formula using loop voltage Method by R.Lundholm

$$Z = 60 \left\{ \ln \left( \frac{2\sqrt{2}h}{r} \right) \right\}$$

- (iv) 1985 - Pointing out about Error of Jordan's Equation by Dr. Okumura of Kyoto University of Japan and Proposal of New Theoretical Equation

$$\begin{aligned} Z &= 60 \left\{ \ln \left( \frac{4h}{r} \right) - 1 \right\} \\ &= 60 \left\{ \ln \left( \frac{2\sqrt{2}h}{r} \right) - 0.653 \right\} \end{aligned}$$

- (v) 1990 - Experimental Formula by Dr. Hara of Kyoto University

$$Z = 60 \left\{ \ln \left( \frac{2\sqrt{2}h}{r} \right) - 2 \right\}$$

- (vi) 1993 - Electromagnetic Field Theory by Takahashi

$$dE = (\mu_0 I_0 c / 4\pi) dx / (ct - x + r_0)^2$$

- (vii) 1995 - Theoretical Formula due to Electromagnetic Field Theory by Takahashi

- (1) In case without ground plane

$$Z = 60 \left\{ \ln \left( \frac{2\sqrt{2}h}{r} \right) - 1.540 \right\}$$

- (2) In case with ground plane

$$Z = 60 \left\{ \ln \left( \frac{2\sqrt{2}h}{r} \right) - 1.983 \right\}$$

From the above it is seen that the first theoretical formulation of tower surge impedance was proposed by Jordan [2]. He assumed that the current distribution inside the tower was uniform from the tower bottom to the top of the tower. However, the effect of return stroke current was neglected. The tower was approximated as a vertical cylinder having a height equal to that of the tower, and a radius equal to the mean equivalent radius of the tower. Propagation velocity inside the tower was assumed to be the velocity of light.



Theoretical formulations of tower surge impedance based on the electromagnetic field theory were proposed by Lundholm *et al.* [3], Wagner and Hileman [4], Sargent and Darveniza [5] and Okumura and Kijima [6], considering effects of the vector potential generated by the injection current into the tower only.

Another experimental value for actual transmission towers was reported by Kawai [7]. He used a direct method to measure tower surge impedance. His experimental results showed that the tower surge response to a vertical current is different from the response to a horizontal current. Measured propagation velocity inside the tower was 70-80% of the velocity of light.

Scale-model measurements were reported by Chisholm [8] [9] and Wahab *et al.* [10]. Chisholm used the time-domain reflectometry (TDR) method to measure tower surge impedance. These measurements were performed using both horizontal and vertical current injection. Measured propagation velocity inside the tower was 80-90% of the velocity of light. These results showed that the tower surge impedance is strongly influenced by the angle of current injection.

Field measurements on full-scale tower impedance using the direct method were reported by Ishii *et al.* and Yamada *et al.* [11]. These measurements were performed using inclined and horizontal current injection. Both of them proposed surge impedance of the tower based on the Electromagnetic Transient Program (EMTP). Propagation velocity inside the tower was assumed to be the velocity of light.

Numerical work was reported by Ishii and Baba [12][13]. They estimated the surge response of a tower by numerical electromagnetic field analysis. The calculated results were compared with the field test results. The analysis showed that surge response and surge impedance of the tower depends on the arrangement of the current lead wire.

Recently experimental and simulation result of the surge impedance of single vertical conductor has been obtained using Finite Difference Time Domain (FDTD) method [14]. Thus, computed and experimental values of surge impedance of single vertical conductor are in well agreement with the theoretical values derived by Takahashi.

### **1.3 Electromagnetic Simulation Technique**

The numerical solution of the electric field integral equations used in Numerical Electromagnetic Code (NEC-2) is first obtained. The measuring method of tower surge impedance are briefly explained and then this effects of the measuring methods and the

arrangements of the measuring wires on the evaluated tower surge impedance are studied by the NEC-2. For the present analysis, the NEC-2 is employed. It is a widely used three dimensional (3-D) electromagnetic modeling code based on the Method of Moments (MoM) in the frequency domain, and is particularly effective in analyzing the electromagnetic response of antennas or of other metallic structures composed of thin wires. A vertical conductor system needs to be decomposed into thin wire elements, and the position, orientation and the radius of each element constitute the input data, along with the description of the source and frequency to be analyzed. In the analysis, all the elements in the systems are treated as perfect conductors. To solve the time varying electromagnetic response, Fourier transform and inverse Fourier transform are used.

The validity of the computed results when NEC-2 is applied to the analysis of surge response of a vertical conductor has been verified by comparing with the theoretical values. Measurements on full-sized towers are straightforward in evaluating the actual characteristics of a tower struck by lightning, however, it is difficult to carry out this kind of experiments in the ideal arrangement where a current lead wire is stretched vertically above the tower top to simulate a lightning channel, owing to its scale. The geometrical arrangement in measurements so far, therefore, has been different from the incident of lightning hitting a tower. Measurements on reduced-scale models are therefore more economical than those on full-sized towers, and are flexible in setting up various experimental arrangements. However, it is not possible to achieve the same accuracy as with the full-scale model. In the measurement by the direct method, the step current is injected into the tower by a pulse generator placed at the tower top, and the voltage between the tower top and a voltage measuring wire is measured. This method is straightforward and the influence of the ground conductivity is automatically incorporated. In the measurement by refraction method wire to guide a rectangular pulse current is connected to the top of a tower under measurement and the refracted or the reflected wave on the measuring wire is observed to evaluate the transient impedance at the tower top. This method is considered valid in evaluating refraction and reflection of surges associated with mid-span strokes or strokes to adjacent towers at the by connecting point of the tower and the earth wires. The tower surge characteristics evaluated this method therefore should be distinguished from those by the direct method.



## 1.4 Electromagnetic Modeling Code

For the accurate analysis of the dynamic electromagnetic field around a vertical conductor struck by lightning, electromagnetic modeling codes are appropriate. Of many available codes, those based on the MoM [15] are probably best suitable for the electromagnetic analysis of a tower system. Since they have widely and successfully been used in analyzing thin-wire antennas or scattering structures, and a tower system can be regarded as a thin-wire antenna. In order to solve the very fast surge phenomena in a 3-D structure tower as an electromagnetic field problem, the FDTD method is also currently available as practical choice. Furthermore, an imperfectly conducting medium is required to be accurately modeled to represent currents in the earth. Comparing the theories of FDTD and MoM, the former is more advantageous to handle 3-D currents in an imperfectly conducting medium such as earth soil without any difficulty, even if the medium is non-homogeneous [16]. On the other hand, the latter is more advantageous to accurately represent the thin wire.

The MoM needs to model only the metal structure of interest, and does not need to model the space around it. Long wires are, therefore, easily modeled. This is the advantage compared with the FDTD Method [17] that may also be applicable to this problem. The MoM requires that the entire structure be divided into wire segments that must be small compared to the wavelength. Once the model is defined, an excitation is imposed as a voltage source or a plane wave on one of the wire segments. The MoM is to determine the current on every segment due to the source and all the other currents by numerically solving the electric field integral equation. Once these currents are known, the electric field at any point in space is determined from the sum of the contributions of all the wire segments. The MoM allows discrete circuit elements to be inserted into a model by simply defining the impedance desired on any given wire segment.

As a MoM-based code, the author uses NEC-2 for the present work. This code was developed at the Lawrence Livermore National Laboratory, California, under the sponsorship of the Naval Ocean Systems Center and the Air Force Weapons Laboratory. Although the latest version is NEC-4 [18], it is available only to the citizens of the United States and Canada, or to the users who are licensed from Lawrence Livermore National Laboratory [19]. Therefore, the author employs NEC-2 developed in 1980 that is now available. The information on the history and availability of the NEC-MoM codes has given in Appendix A.



## 1.5 The Objectives of the Research:

Conventional surge problems have successfully been solved by circuit theory, where transmission lines consisting of wires parallel to the earth surface are modeled by distributed-parameter circuit elements and the other components by lumped parameter circuit elements. The distributed parameter circuit theory assumes plane wave propagation that is a reasonable and accurate approximation for the transmission lines, and this assumption enable handling of the electromagnetic wave propagation within the circuit theory. On the other hand, very fast surge phenomena in a 3-D structure, which includes surge propagation in a transmission tower and in a tall building, cannot be approximated by plane wave propagation. Thus, those phenomena cannot be dealt with by circuit theory but need to be solved by Maxwell's equation as an electromagnetic field problem. Nowadays, the surge propagation through a transmission tower needs to be analyzed for economical insulation design. It is also important to assess the interference of lightning surges with information devices inside the building. The surge simulation results using NEC-2 of a vertical conductor are presented in this work. The application of NEC-2 code is discussed for two cases (with the effect of ground plane and without ground plane) of current injection into the vertical conductor. To validate the accuracy and to compare with the theoretical values the results obtained in the NEC-2 have been taken into account. A numerical electromagnetic simulation has been carried out to obtain the various sorts of characteristics of lightning surge response on a vertical tower model. The expected result relates the followings:

- (i) Surge impedance measurement.
- (ii) Influence of ground plane on vertical conductor.
- (iii) Effect of lightning return stroke (direct stroke).
- (iv) Effect of stroke to mid span between towers (indirect stroke).
- (v) Dynamic electromagnetic behavior, especially transient response.
- (vi) Comparison of simulation result using NEC-2 with the recently developed theoretical values.
- (vii) Verification of NEC-2 for actual tower.
- (viii) Surge impedance analysis for an actual tower.

In fine, the purpose of this work are to clarify the surge characteristics of a reduced scale vertical conductor model as well as four parallel conductors model equivalent to real tower structure by analyzing the electromagnetic field around it with the help of NEC-2 based on MoM considering with the effect of with ground plane and without ground plane.



## Chapter 2

# Application of NEC-2 Code to the Analysis of Tower Surge Response

### 2.1 Introduction

For practical purposes the analysis of lightning transients in large conducting structures has mostly been made through modeling the structure by transmission lines. In this approach the parameters of a transmission lines such as the surge impedance, the velocity of the travelling wave etc. need to be determined. This is physically correct if the electromagnetic field around a conductor is in the TEM mode, in that the distribution of the electric field is the same as the electrostatic field. Parameters of the modeled transmission line for parallel conductors or a horizontal conductor above a ground plane can be determined on physical basis.

The electric field around a non-parallel conductor or a non-horizontal conductor above a ground plane is not in the TEM mode during transient periods. In modeling such conductor systems by transmission lines, their parameter needs to be determined. Electromagnetic field around a conductor system needs to be solved to produce induced voltage and distribution of currents through the structure.

The purpose of this chapter is to demonstrate the validity and the accuracy of NEC-2 when it is applied to the electromagnetic field analysis of tower surge response [20]-[26]. NEC-2 code, a standard tool for numerical analysis on electromagnetic field around antennas, can be applied to analysis of lightning transient overvoltages. This code solves 3-D boundary problems by using the electric field integral equation (EFIE).

The EFIE used in NEC-2, its derivation and the numerical method are first outlined in this chapter. Guidelines for modeling structures with this code are mentioned. Finally the applicability of NEC-2 to the transient analysis of the surge impedance of vertical conductor as well as transmission tower, including the effects of ground plane and without ground plane are verified by comparing the simulation result with the theoretical formula.

### 2.2 Electric Field Integral Equation

NEC-2 allows to use both the electric field integral equation and the magnetic field integral equation. The former is suited for analysis of thin-wire structures, while the latter is



suitable for structures having large smooth surfaces. The former can be used to analyze voluminous structures by representing surface with wire grids. In the application to time-domain analysis, the modeling by using thin wires has been employed throughout. The following description on the basic theory of NEC-2 is extract from the program description. The form of electric field integral equation used in NEC-2 follows from an integral representation for the electric field of a volume current distribution  $J_v$ ,

$$E(r) = \frac{-j\eta}{4\pi k} \int_V J_v(r') \cdot \overline{\overline{G}}(r, r') dV', \quad (2.1)$$

where

$$\overline{\overline{G}}(r, r') = (k^2 \overline{\overline{I}} + \nabla \nabla) g(r, r'),$$

$$g(r, r') = \exp(-jk|r - r'|) / |r - r'|,$$

$$k = \omega \sqrt{\mu_0 \epsilon_0}, \eta = \sqrt{\mu_0 / \epsilon_0}$$

and the time convention is  $\exp(j\omega t)$ .  $\overline{\overline{I}}$  is the identity dyad ( $\hat{x}\hat{x} + \hat{y}\hat{y} + \hat{z}\hat{z}$ ). Where  $\mu_0$  and  $\epsilon_0$  are the permeability and permittivity of the free space respectively,  $k$  is the wave number,  $\eta$  is the intrinsic impedance which has a value of  $120\pi$  in the free space and  $\omega$  is the angular frequency. When the current distribution is limited to the plane of a perfectly conducting body, equation (2.1) becomes

$$E(r) = \frac{-j\eta}{4\pi k} \int_S J_s(r') \cdot \overline{\overline{G}}(r, r') dS', \quad (2.2)$$

with  $J_s$  the surface current density. The observation point  $r$  is restricted to be off the surface  $S$  so that  $r \neq r'$ . If  $r$  approaches  $S$  as a limit equation (2.2) becomes

$$E(r) = \frac{-j\eta}{4\pi k} \oint_S J_s(r') \cdot \overline{\overline{G}}(r, r') dS', \quad (2.3)$$

where the principal value  $\oint$  is indicated since  $g(r, r')$  is now unbounded.

An integral equation for the current induced on  $S$  by an incident field  $E_{inc}$  can be obtained from equation (2.3) and the boundary condition for  $r \in S$ ,

$$n(r) \times [E_{scat}(r) + E_{inc}(r)] = 0, \quad (2.4)$$

where  $n(r)$  is the unit normal vector of the surface at  $r$  and  $E_{scat}$  is the field due to induced current  $J_s$ . Substituting equation (2.3) for  $E_{scat}$  yields the integral equation,

$$-n(r) \times E_{inc}(r) = \frac{-j\eta}{4\pi k} n(r) \times \oint_S J_s(r') \cdot (k^2 \overline{\overline{I}} + \nabla \nabla) g(r, r') dS' \quad (2.5)$$



The vector integral in equation (2.5) can be reduced to a scalar integral equation when the conducting surface  $S$  is that of a cylindrical thin wire, thereby making the solution much easier. The assumptions applied to a thin-wire, known as thin-wire approximation, are as follows:

- (i) Transverse currents relative to axial currents on the wire can be neglected.
- (ii) The circumferential variation in the axial current can be neglected.
- (iii) The current can be represented by a filament on the wire axis.
- (iv) The boundary conditions on the electric field need to be enforced in the axial direction only.

These assumptions are valid as far as the wire radius is much less than the wavelength and much less than the wire length. From 1<sup>st</sup>, 2<sup>nd</sup> and 3<sup>rd</sup> assumptions, the surface current density  $J_s$  on a wire of a radius 'a' can be replaced by a filamentary current  $I$ ,

$$I(s)\hat{s} = 2\pi a J_s(r)$$

where  $s$  is the distance parameter along the wire axis at  $r$  and  $\hat{s}$  is the unit vector tangent to the wire axis at  $r$ .

Equation (2.5) then becomes

$$-n(r) \times E_{inc}(r) = \frac{-j\eta}{4\pi k} n(r) \times \int_L I(s')(k^2 \hat{s}' - \nabla \frac{\partial}{\partial s'}) g(r, r') ds', \quad (2.6)$$

where the integration is over the length of the wire. Enforcing the boundary condition in the axial direction reduces equation (2.6) to a scalar equation,

$$-\hat{s} \cdot E_{inc}(r) = \frac{-j\eta}{4\pi k} \int_L I(s')(k^2 \hat{s} \cdot \hat{s}' - \frac{\partial^2}{\partial s \partial s'}) g(r, r') ds', \quad (2.7)$$

since  $r'$  is now the point at  $s'$  on the wire axis while  $r$  is a point at  $s$  on the wire surface  $|r - r'| \geq a$  and the integrand is bounded.

This is the basic electric field integral equation at the surface of a thin conducting wire in the axial direction reduced to the scalar equation under the restriction of the boundary condition given by equation (2.4) in the axial direction.

The electric field integral equation is easily extended to imperfect conductors by modifying the boundary condition from equation (2.4) to

$$n(r) \times [E_{scat}(r) + E_{inc}(r)] = Z_s(r) [n(r) \times J_s(r)] \quad (2.8)$$

where the  $Z_s(r)$  is the surface impedance at  $r$  on the conducting surface. For a wire, the boundary condition is

$$\hat{s} \cdot [E_{scat}(r) + E_{inc}(r)] = Z_L(s) I(s) \quad (2.9)$$

where,  $Z_L(s)$  is the impedance per-unit length at  $s$ .

### 2.3 Numerical Solution by the Method of Moments

The integral equation (2.7) is solved numerically in NEC-2 by the Method of Moments. This method applies to a general linear-operator equation,

$$Lf = e \quad (2.10)$$

where  $f$  is an unknown response,  $e$  is a known excitation, and  $L$  is a linear operator (an integral operator in the present case). The unknown function  $f$  may be expanded in a sum of basis functions,  $f_j$ , as

$$f \cong \sum_{j=1}^N \alpha_j f_j \quad (2.11)$$

A set of equations for the coefficients  $\alpha_j$  are then obtained by taking the inner product of equation (2.10) with a set of weighting functions,  $\{w_i\}$ ,

$$\langle w_i, Lf \rangle = \langle w_i, e \rangle \quad i = 1, 2, \dots, N. \quad (2.12)$$

Due to the linearity of  $L$ , equation (2.11) substituted for  $f$  yields,

$$\sum_{j=1}^N \alpha_j \langle w_i, Lf_j \rangle = \langle w_i, e \rangle \quad i = 1, 2, \dots, N. \quad (2.13)$$

This equation can be written in matrix form as

$$[G][A] = [E], \quad (2.14)$$

where  $G_{ij} = \langle w_i, Lf_j \rangle$ ,  $A_j = \alpha_j$ ,  $E_i = \langle w_i, e \rangle$ , and is easily solved.

The solution is then  $[A] = [G]^{-1}[E]$ .

For the solution of equation (2.7), the inner product is defined as

$$\langle f, g \rangle = \int_S f(r)g(r)dS,$$

where the integration is over the structure surface. Various choices are possible for the weighting function  $\{w_i\}$  and basis functions  $\{f_i\}$ . When  $w_i = f_i$ , the procedure is known as Galerkin's method. In NEC-2, the basis and weighting functions are different, and  $\{w_i\}$  are chosen as a set of delta functions

$$w_i(r) = \delta(r - r_i),$$

with  $\{r_i\}$  a set of points on the conducting surface. The result is a point sampling of the integral equations known as the collocation method of solution. Wires are divided into short straight segments with a sample point at the center of each segment.

The choice of basis functions is very important for an efficient and accurate solution. In NEC-2, the support of  $f_i$  is restricted to a localized subsection of the surface near  $\{r_i\}$ . This choice simplifies the evaluation of the inner-product integral and ensures that the matrix  $G$  will be well conditioned. For finite  $N$ , the sum of  $f_i$  cannot exactly equal to a general current distribution. Wires in NEC-2 are modeled by short straight segments with current on each segment represented by three terms a constant sine function and a cosine function. This expansion has been shown to provide rapid solution convergence. It has the added advantage that the fields of the sinusoidal currents are easily evaluated in a closed form. The amplitudes of the constant, sine and cosine terms are related such that their sum satisfies physical conditions on the local behavior of current and charge at the segment ends.

The total current on segment number  $j$  in NEC-2 has the form or the current expansion functions in NEC-2 have the form

$$I_j = A_j + B_j \sin k(s - s_j) + C_j \cos k(s - s_j), \quad (2.15)$$

$$|s - s_j| < \frac{\Delta_j}{2},$$

where,  $k = \omega \sqrt{\mu_0 \epsilon_0}$ , where  $s_j$  is the value of  $s$  at the center of segment  $j$  and  $\Delta_j$  is the length of segment  $j$ . Of the three unknown constants  $A_j$ ,  $B_j$  and  $C_j$ , two are eliminated by local conditions on the current leaving one constant, related to the current amplitude, to be determined by the matrix equation. The local equations are applied to the current and to the linear charge density,  $q$ , which is related to the current by the equation of continuity

$$\frac{\partial I}{\partial s} = -j\omega q. \quad (2.16)$$

At a junction of two segments with uniform radius, the obvious condition is that the current and charge are continuous at the junction. At a junction of two or more segments with unequal radii, the continuity of current is generalized to Kirchhoff's current law that the algebraic sum of current into the junction is zero. The total charge in the vicinity of the junction is assumed to distribute itself on individual wires according to the wire radii, neglecting local coupling effects.



The solution requires the evaluation of electric field at each segment due to this current. Three approximations of the integral equation kernel are used:

- (i) a thin-wire form for most cases
- (ii) an extended thin-wire form for thick wires and
- (iii) a current element approximation for large interaction distance

In each case the evaluation of the field is greatly simplified by the use of formulas for the fields of the constant and sinusoidal current components. Studies have been carried out considering the thin-wire kernel.

The accuracy of the thin-wire kernel approximation for a wire of radius ' $a$ ' and length ' $\Delta L$ ' depends on  $ka$  and  $\Delta L / a$ . Studies have shown that the thin-wire approximation leads to error of less than 1% for  $\Delta L / a$  greater than 8. Furthermore, in the numerical solution of Electric Field Integral Equation (EFIE), the wire is divided into segments less than about  $0.1\lambda$  in length to obtain the adequate representation of current distribution thus restricting  $ka$  to less than about 0.08.

For the thin-wire kernel, the source current is approximated by a filament on the segment axis while the observation point is on the surface of the observation segment. The fields are evaluated with the segment on the axis of a local cylindrical co-ordinate system as illustrated in Fig. 2.1 below [19]:

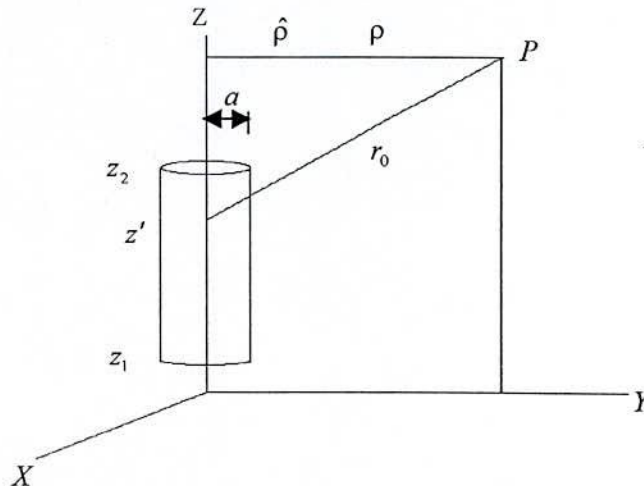


Figure 2.1: Current Filament Geometry for Thin-Wire Kernel.

Then with

$$G_0 = \exp(-jkr_0)/r_0 \text{ and } r_0 = [\rho^2 + (z - z')^2]^{1/2},$$

the  $\rho$  and  $z$  components of the electric field at  $P$  due to a sinusoidal current filament of arbitrary phase,

$$I = \sin(kz' - \theta_0), \quad z_1 < z' < z_2,$$

$$\text{are } E_\rho^f(\rho, z) = \frac{-jn}{2k^2\lambda\rho} \left[ (z' - z)I \frac{\partial G_0}{\partial z'} + IG_0 - (z' - z)G_0 \frac{\partial I}{\partial z'} \right]_{z_1}^{z_2}, \quad (2.17)$$

$$E_z^f(\rho, z) = \frac{jn}{2k^2\lambda} \left[ G_0 \frac{\partial I}{\partial z'} - I \frac{\partial G_0}{\partial z'} \right]_{z_1}^{z_2}. \quad (2.18)$$

For a current that is constant over the length of the segment with strength  $I$ , the fields

$$\text{are } E_\rho^f(\rho, z) = \frac{I}{\lambda} \frac{jn}{2k^2} \left[ \frac{\partial G_0}{\partial \rho} \right]_{z_1}^{z_2}, \quad (2.19)$$

$$E_z^f(\rho, z) = \frac{I}{\lambda} \frac{jn}{2k^2} \left\{ \left[ \frac{\partial G_0}{\partial z'} \right]_{z_1}^{z_2} + k^2 \int_{z_1}^{z_2} G_0 dz' \right\}. \quad (2.20)$$

These field expressions are exact for the specified currents. The integral over  $z'$  of  $G_0$  is evaluated numerically in NEC. Substituting sine and cosine currents and evaluating the derivatives yields the following equation for the fields. For

$$I = I_0 \begin{pmatrix} \sin kz' \\ \cos kz' \end{pmatrix},$$

$$E_\rho^f(\rho, z) = \frac{-I_0}{\lambda} \frac{j\eta}{2k^2\rho} G_0 \left\{ k(z - z') \begin{pmatrix} \cos kz' \\ -\sin kz' \end{pmatrix} + \left[ 1 - (z - z')^2 (1 + jkr_0) \frac{1}{r_0^2} \right] \begin{pmatrix} \sin kz' \\ \cos kz' \end{pmatrix} \right\}_{z_1}^{z_2},$$

$$E_z^f(\rho, z) = \frac{I_0}{\lambda} \frac{j\eta}{2k^2} G_0 \left\{ k \begin{pmatrix} \cos kz' \\ -\sin kz' \end{pmatrix} + \left[ (1 + jkr_0)(z - z') \frac{1}{r_0^2} \right] \begin{pmatrix} \sin kz' \\ \cos kz' \end{pmatrix} \right\}_{z_1}^{z_2}$$

For a constant current of strength  $I_0$ ,

$$E_\rho^f(\rho, z) = \frac{-I_0}{\lambda} \frac{j\eta\rho}{2k^2} \left[ (1 + jkr_0) \frac{G_0}{r_0^2} \right]_{z_1}^{z_2}, \quad (2.21)$$

$$E_z^f(\rho, z) = \frac{-I_0}{\lambda} \frac{j\eta}{2k^2} \left[ (1 + jkr_0)(z - z') \frac{G_0}{r_0^2} \right]_{z_1}^{z_2} - \frac{I_0}{\lambda} \frac{j\eta}{2k^2} k^2 \int_{z_1}^{z_2} G_0 dz'. \quad (2.22)$$

Despite the seemingly crude approximation, the thin wire kernel does accurately represent the effect of wire radius for wires that are sufficiently thin.

## 2.4 Structure Modeling Guideline

The basic devices for modeling structures with the NEC code are short, straight segments for modeling wires and flat patches for modeling surfaces. An antenna and any other conducting objects in its vicinity that affect its performance must be modeled with strings of segments following the paths of wires and with patches covering surfaces. Proper choice of the segments and patches for a model is the most critical step to obtaining accurate results. The number of segments and patches should be the minimum required for accuracy, however, since the program running time increases rapidly this number increases. Guidelines for choosing segments and patches are given below and should be followed carefully by anyone using the NEC code. Experience gained by using the code will also aid the user in developing models.

A wire segment is defined by the coordinates of its two end points and its radius. Modeling a wire structure with segments involves both geometrical and electrical factors. Geometrically, the segments should follow the paths of conductors as closely as possible, using a piece-wise linear fit on curves.

The main electrical consideration is segment length  $\Delta L$  relative to the wavelength  $\lambda$ . Generally,  $\Delta L$  should be less than about  $0.1\lambda$  at the desired frequency. Somewhat longer segments may be acceptable on long wires with no abrupt changes while shorter segments,  $0.05\lambda$  or less, may be needed in modeling critical regions of an antenna. The size of the segments determines the resolution in solving for the current on the model since the current is computed at the center of each segment. Extremely short segments, less than about  $10^{-3}\lambda$ , should also be avoided since the similarity of the constant and cosine components of the current expansion leads to numerical inaccuracy.

The wire radius,  $a$ , relative to  $\lambda$  is limited by the approximations used in the kernel of the electric field integral equation. Two approximation options are available in NEC-2: the thin-wire kernel and the extended thin-wire kernel. In the thin-wire kernel, the current on the surface of a segment is reduced to a filament of current on the segment axis. In the extended thin-wire kernel, a current uniformly distributed around the segment surface is assumed. The field of the current is approximated by the first two terms in a series expansion of the exact field in powers of  $a^2$ . The first term in the series, which is independent of  $a$ , is identical to the thin-wire kernel while the second term extends the accuracy for larger values of  $a$ . Higher order approximation are not used because they would require excessive computation time.



In either of these approximations, only currents in the axial direction on a segment are considered, and there is no allowance for variation of the current around the wire circumference. The acceptability of these approximations depends on both the value of  $a/\lambda$  and the tendency of the excitation to produce circumferential current or current variation. Unless  $2\pi a/\lambda$  is much less than 1, the validity of these approximations should be considered.

The accuracy of the numerical solution for the dominant axial current is also dependent on  $\Delta L/a$ . It must be greater than about 8 to limit errors less than 1%, since small values of  $\Delta L/a$  may result in extraneous oscillations in the computed current near free wire ends, voltage sources, or lumped loads. Use of the extended thin-wire kernel will extend the limit on  $\Delta L/a$  to smaller values than are permissible with the normal thin-wire kernel. Studies of the computed field on a segment due to its own current have shown that with the thin-wire kernel, with the extended thin-wire kernel,  $\Delta L/a$  may be as small as 2 for the same accuracy. In the current solution with either of these kernels, the error tends to be less than for a single field evaluation. Reasonable current solutions have been obtained with the thin-wire kernel for  $\Delta L/a$  down to about 2 and with the extended thin-wire kernel for  $\Delta L/a$  down to 0.5. When a model includes segments with  $\Delta L/a$  less than about 2, the extended thin-wire kernel option should be used by inclusion of an 'EK' card in the data deck. When the extended thin-wire kernel option is selected, it is used at free wire ends and between parallel, connected segments. The normal thin-wire kernel is always used at bends in wires, however. Hence, segments with small  $\Delta L/a$  should be avoided at bends. Use of a small  $\Delta L/a$  at a bend, which results in the center of one segment falling within the radius of the other segment, generally leads to severe error.

The current expansion used in NEC enforces conditions on the current and charge density along wires, at junctions, and at wire ends. For these conditions to be applied properly, segments that are electrically connected must have coincident end points. If segments intersect other than at their ends, the NEC-2 code will not allow current to flow from one segment to the other. Segments will be treated as connected if the separation of their ends is less than about  $10^{-3}$  times the length of the shortest segment. When possible, however, identical coordinates should be used for connected segment ends.

The angle of the intersection of wire segments in NEC-2 is not restricted in any manner. In fact, the acute angle may be so small as to place the observation point on one wire segment within the volume of another wire segment. Numerical studies have shown that such

overlapping leads to meaningless results; thus, as a minimum, one must ensure that the angle is large enough to prevent overlaps. Even with such care, the details of the current distribution near the intersection may not be reliable even though the results for the current may be accurate at distances from this region.

Wire-grid modeling of conducting surfaces has been used with varying success. The earliest applications to the computation of radar cross sections and radiation patterns provided reasonably accurate results. Even computations for the input impedance of antennas driven against grid models of surfaces have often times exhibited good agreement with experiments. However, broad and generalized guidelines for near-field quantities have not been developed, and the use of wire-grid modeling for near-field parameters should be approached with caution. A single wire grid, however, may represent both surfaces of a thin conducting plate. The current on the grid will be the sum of the currents that would flow on opposite sites of the plate. While information on the currents on the individual surfaces is lost the grid will yield the correct radiated fields.

Other rules for the segment model follows:

- (i) Segments (or patches) may not overlap since the division of current between two overlapping segments is indeterminate. Overlapping segments may result in a singular matrix equation.
- (ii) A large radius change between connected segments may decrease accuracy; particularly, with small  $\Delta L/a$ . The problem may be reduced by making the radius change in steps over several segments.
- (iii) A segment is required at each point where a network connection or voltage source will be located. This may seem contrary to the idea of an excitation gap as a break in a wire. A continuous wire across the gap is needed, however, so that the required voltage drop can be specified as a boundary condition.
- (iv) The two segments on each side of a charge density discontinuity voltage source should be parallel and have the same length and radius. When this source is at the base of a segment connected to a ground plane, the segment should be vertical.
- (v) The number of wires joined at a single junction cannot exceed 30 because of a dimension limitation in the code.
- (vi) When wires are parallel and very close together, the segments should be aligned to avoid incorrect current perturbation from offset match point and segment junctions.
- (vii) Although extensive tests have not been conducted, it is safe to specify that wires should be several radii apart.



## 2.5 Example of input data

The sample input data deck to NEC-2, which is for an impulse voltage measuring system as illustrated in the following Fig. 2.2, is shown in the following table 1. For this example, the resistor divider of 3.3 m in height is divided into 6 segments of 0.55 m.

The input data deck must begin with comment lines 'CM'. The comment lines are terminated by 'CE'. A line starting with 'GW' represents a cylindrical straight wire. The number next to 'GW' is a tag number assigned to all segments of wire. The one next to it is the number of segments into which the wire is divided. The decimal numbers next to them are the coordinates of the wire ends and the radius of the wire  $(x_1, y_1, z_1, x_2, y_2, z_2, a)$ . Note that the unit is in meters.

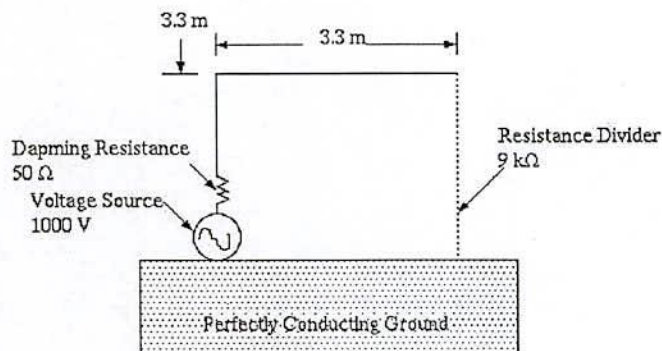


Figure 2.2: An impulse voltage measuring system subjected to analysis as example.

Table 1: Sample input data to NEC-2:

```

CM IMPULSE VOLTAGE MEASURING SYSTEM
CM N=512 Delta T= 2.5E-09 SEC
CE PERFECTLY CONDUCTING GROUND IS USED
GW 1 6 0.0 0.0 0.0 0.0 0.0 3.3 0.0025
GW 2 6 0.0 0.0 3.3 3.3 0.0 3.3 0.0025
GW 3 6 3.3 0.0 3.3 3.3 0.0 0.0 0.0025
GE 1
GN 1
LD 4 1 2 2 50.0
LD 4 3 1 6 1500.0
FR 0 257 0 0 7.813E-01 7.813E-01
EX 0 1 1 00 1000.0 0.0
PT 0 3 6
XQ
EN

```



The following two lines, 'GE 1' and 'GN 1', indicate a perfectly conducting ground exists at  $z = 0$ , i.e. by this commands, images below ground are generated. The 9<sup>th</sup> and 10<sup>th</sup> lines beginning with 'LD' specify the impedance loading. The 9<sup>th</sup> line indicates that the second segment of the set of segments whose tag number is 1 is loaded by resistance of  $50 \Omega$ . Similarly, the 10<sup>th</sup> line indicates that each of the 1<sup>st</sup> segments through 6<sup>th</sup> segments of the set of segments having tag number of 3 is loaded by  $1500 \Omega$ , respectively.

In the line starting with 'FR', the frequency range is specified as 0.7813 MHz to 200 MHz with the linear increment step of 0.7813 MHz. In the line of 'EX', the excitation for the structure is specified. In this case, a voltage source generating 1000 volts is inserted into the 1<sup>st</sup> segment of the set of segments having tag number of 1. By the line beginning with 'PT', currents for the 6<sup>th</sup> segment of the set of segments whose tag number is 3 are printed. The last two commands: 'XQ' and 'EN' are commands of program execution and end, respectively.

For the present analysis, the author uses  $\Delta t = 0.25$  ns. So according to the modeling guideline of NEC-2 the frequency will be as follows:

$$\text{Frequency } f = \frac{1}{512 \times \Delta t} \text{ MHz} = \frac{1}{512 \times 0.25 \times 10^{-9}} \text{ MHz} = 7.8125 \text{ MHz}$$

Now the wavelength  $\lambda = \frac{c}{f}$ , where  $c$  is the velocity of light and  $f$  is the frequency.

$$\text{So, the wavelength } \lambda = \frac{3 \times 10^8}{7.8125 \times 10^6} \text{ meter} = 38.4 \text{ meter}$$

Now the value of  $\Delta L$  must be within  $10^{-3} \lambda \leq \Delta L \leq 0.1 \lambda$ . Here, the limiting range for  $\Delta L$  becomes  $0.0384 \text{ m} \leq \Delta L \leq 3.84 \text{ m}$  or  $3.84 \text{ cm} \leq \Delta L \leq 3.84 \text{ m}$ . Conventionally, the author uses  $\Delta L = 10 \text{ cm}$ , which is within the limit.

When modeling complex structures with features not previously encountered, accuracy may be checked by comparison with reliable experimental data if available. Alternatively, it may be possible to develop an idealized model for which the correct results can be estimated while retaining the critical features of the desired model. The optimum model for a class of structures can be estimated by varying the segment and patch density and observing the effect on the results. Some dependence of results on segmentation will always be found. A large dependence, however, would indicate that the solution has not converged and more segments or patches should be used. A model will generally be usable over a band of frequencies. For frequencies beyond the upper limit of a particular model, a new set of

geometry cards must be input with a finer segmentation.

Several options are available in NEC-2 for modeling an antenna over a ground plane. For a perfectly conducting ground, the code generates an image of the structure reflected in the ground surface. The image is exactly equivalent to a perfectly conducting ground and results in solution accuracy comparable to that for a free-space model. Structures may be close to the ground or contacting it in this case. However, for a horizontal wire with radius  $a$ , and height  $h$  to the wire axis,  $[h^2 + a^2]^{1/2}$  should be greater than about  $10^6$  wavelengths. Furthermore, the height should be at least several times the radius for the thin-wire approximation to be valid.

A finitely conducting ground can be modeled by Sommerfeld-Norton approximation. It should be noted that NEC-2 can model wires over lossy ground but it cannot model wires buried in the ground. Although NEC-4, the latest version of the NEC-MoM codes, can model buried wires.

## 2.6 Theoretical Formula of Surge Impedance

There is a theoretical formula of surge impedance of a vertical conductor, in case with ground plane and without ground plane. Suppose that lightning surge strike on the vertical conductor whose height is  $h$  and radius is  $r$ . Then the surge current wave is reflected at the ground of the perfect conductor and returns to the top of the vertical conductor.

Introducing the current reflectivity  $\beta = 1$  and the magnetic field reflectivity  $\gamma(\gamma_i, \gamma_r) = 0$ , the theoretical formula of surge impedance, which is very close to the well-known empirical formula of Dr. Hara

$$Z = 60 \left\{ \ln \left( \frac{2\sqrt{2}h}{r} \right) - 2 \right\}, \quad (2.23)$$

is obtained as follows:

$$\begin{aligned} Z &= 60 \left( \ln \left( \frac{h}{2r} \right) - \frac{1}{4} \right); \\ &= 60 \left( \ln \left( \frac{2\sqrt{2}h}{r} \right) - 1.983 \right). \end{aligned} \quad (2.24)$$

Equation (2.24) gives the surge impedance of the vertical conductor just after the occurrence of the reflection of the traveling wave propagation down from the top of the structure. However if it is considered that  $\beta = \gamma_i = \gamma_r = 1$ , the potential  $V(t)$  generated in the vertical conductor at  $h$  became,



$$V(t) = \frac{c\mu_0 I_0}{2\pi} \left( \ln \frac{(ct + 2r)}{2r} - \frac{ct}{2(ct + r)} \right).$$

The above equation can be modified by substituting  $ct = 2h$ , where  $c$  is the velocity of light and assuming  $h \gg r$  as follows:

$$\begin{aligned} Z &= 60 \left( \ln \left( \frac{h}{r} \right) - \frac{1}{2} \right) \\ &= 60 \left( \ln \left( \frac{2\sqrt{2}h}{r} \right) - 1.540 \right). \end{aligned} \quad (2.25)$$

On the other hand, if there is no ground, the following formula is induced

$$\begin{aligned} V(t) &= \int_0^{ct} (-E_i \cdot dl) \\ &= \frac{c\mu_0 I_0}{2\pi} \left( \ln \frac{(ct + 2r)}{2r} - \frac{ct}{2(ct + r)} \right) \end{aligned}$$

Substituting  $ct = 2h$  and assuming  $h \gg r$  in the above equation, we get

$$\begin{aligned} Z &= 60 \left( \ln \left( \frac{h}{r} \right) - \frac{1}{2} \right) \\ &= 60 \left( \ln \left( \frac{2\sqrt{2}h}{r} \right) - 1.540 \right). \end{aligned} \quad (2.26)$$

This formula given by equation (2.26) is the same as equation (2.25). Then, we calculate the value of surge impedance by these equation and compare with NEC-2 results comparing with and without ground plane.

## 2.7 Application to the Analysis of Vertical Conductor Surge Response

The analysis of transient behavior of tower struck by lightning is an important problem when studying the lightning performance of transmission lines. The issue has gained more importance with the recent use of instrumented telecommunication towers to capture lightning return stroke currents, also in power system equipment (circuit breakers, disconnects, control and protection circuits), and in household appliances has increases the interest of transients. From this point of view, transient caused by lightning (direct and or indirect) can be one of the major causes of malfunction, or even destruction of electrical equipments. Direct lightning may be defined as a lightning stroke, which directly hits a line, connected to the installation or the equipment. On the other hand, Indirect if the strike is at a certain distance and the currents are induced by the electromagnetic field generated by the



lightning discharge. In this research, if the lightning current channel does not terminate then it has been denoted as without ground plane and vice-versa.

This section describes the numerical simulation of the surge response of a vertical conductor, including the effects of ground plane and without ground plane [20]-[24]. NEC-2 is applied to the electromagnetic field analysis of vertical conductor surge response.

For the analysis different reduced scale model of vertical conductor were taken such as 60 cm, 90 cm and 120 cm of height. Fig. 2.3 shows reduced-scale of 60 cm model of the single vertical conductor system for the surge analysis. The arrangement of the current lead wire connected to the top of the vertical conductor with the existence of ground plane and without ground plane is indicated in Fig. 2.3 and Fig. 2.4 respectively. Whereas, Fig. 2.3 simulates a lightning stroke to mid-span and also have been called the refraction method.

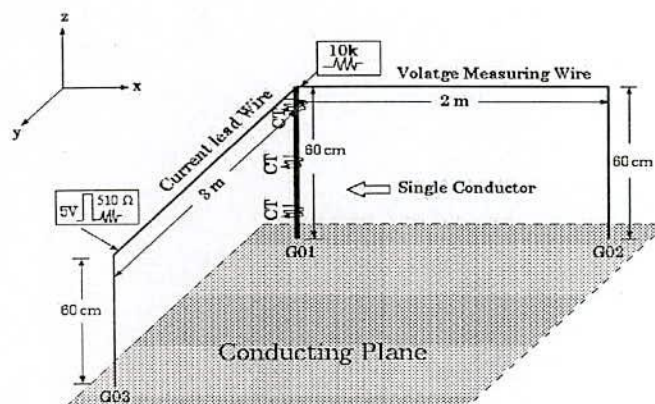


Figure 2.3: Arrangement of the vertical conductor system for the simulation using NEC-2 with ground plane.

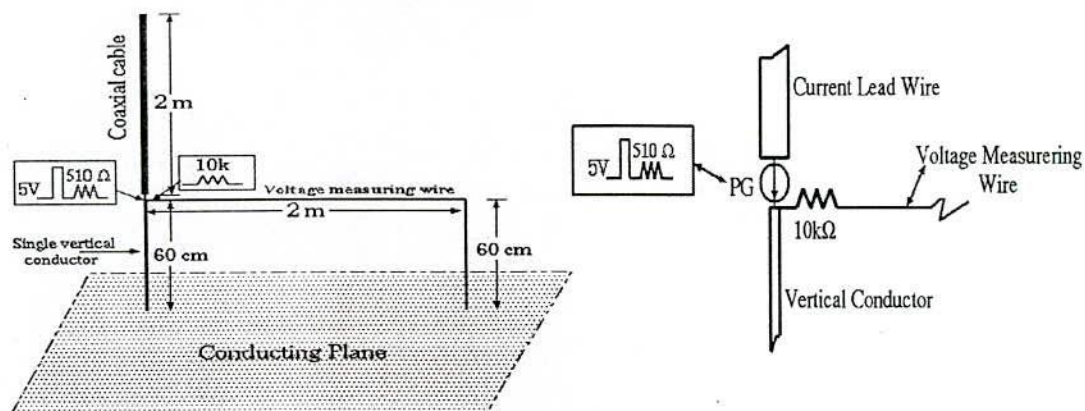


Figure 2.4: Arrangement of the vertical conductor system for the simulation using NEC-2 without ground plane.

Fig. 2.4 also illustrates an arrangement for analysis, which simulates a vertical lightning stroke hitting a tower top [25][26]. In this type of analysis, two kinds of lightning strokes are simulated: one is a return stroke and the other is a downward traveling current wave.

In the case of a return stroke to a tower, a downward leader, which is similar to a charged vertical transmission line whose lower end is open, contacts the top of the tower. This situation can be simulated by placing a pulse current generator at the tower top. Another type of the lightning phenomena caused by a downward traveling current wave can also be examined. In such kinds of strokes, a current wave is thought to propagate down the lightning channel from the cloud to the tower top. For the simulation of this situation, a pulse current generator needs to be placed remotely above the channel. However, the computed waveforms for this case of current injection, a current wave traveling down the current lead wire, are similar to those of return stroke type without the influence of the finite length of the wire.

A voltage measuring wire of 200 cm in length is placed perpendicular to the current lead wire and is connected to the top of the vertical conductor, which is 60 cm in height, and radius of 0.05 cm. The ends of the horizontal voltage measuring wire in both cases are stretched down and connected to the ground through matching resistance. If the electromagnetic wave inside the vertical conductor system travels at the velocity of light, this termination condition does not affect the phenomena at the vertical conductor within 13.33 ns.

A step current pulse generator having pulse voltage of 5 V in magnitude, rise-time of 1 ns and pulse width of 40 ns is installed in both cases which is meant to incorporate the influence of the induction from the lightning channel hitting the vertical conductor. Fig. 2.5 shows the waveforms of the injected current for the simulation using NEC-2.

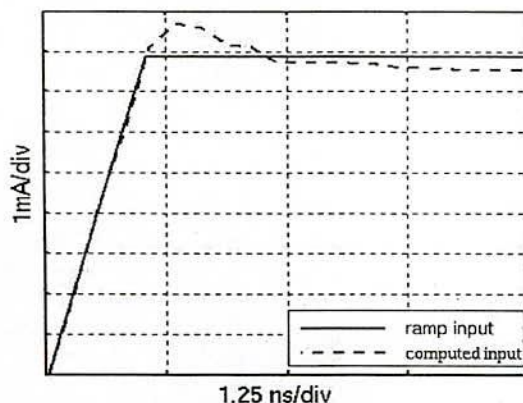


Figure 2.5: Waveform of the injected current.



Since NEC-2 is a computer code in the frequency domain, the Fourier transform and the inverse Fourier transform are used to solve the time-varying electromagnetic fields.

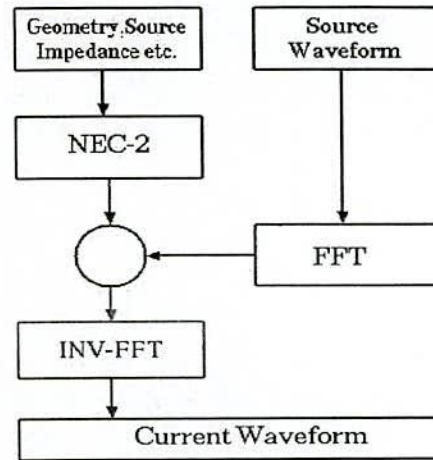


Figure 2.6: Flowchart of the solution using NEC-2.

The flowchart of the NEC-2 solution is shown in Fig. 2.6. For the numerical analysis, the conductor system needs to be modeled with segments according to the modeling guidelines stated in the preceding section. To save the computation time, the conductors of the system are divided into 10 cm segments in this work. This segmentation must satisfy electrical consideration relative to the wavelength as:

$$10^{-3} \lambda \leq \Delta L \leq 0.1 \lambda$$

This requirement is too severe to be satisfied exactly, since wider frequency range is needed to investigate the transient characteristics of such a system.

To evaluate the voltage of the top of a structure, 10 k $\Omega$  resistance was inserted between the top of the structure and the end of the voltage measuring wire. Input data for NEC-2 program is given in Appendix-B. The voltage at the top of vertical conductor through the horizontal voltage measuring wire is obtain and also the waveform of current flowing through the vertical conductor is obtained from the simulation. The system of structures under the analyses was postulated to be on the perfectly conducting ground of Copper with conductivity  $5.8 \times 10^7$  mho/meter. Then we calculate the surge impedance, by the recently developed formula [27], which is defined by the ratio of the instantaneous values of the voltage to the current at the moment of voltage peak.

As the pulse applied to the current lead wire according to Fig. 2.7, the current starts flowing through the vertical conductor instantly. However, for the arrangement as shown in



Fig. 2.3, the current through the vertical conductor is delayed by the round-trip time of the travelling wave in the conductor. While in both cases, the reflection wave from the ground reaches the top of the vertical conductor at  $t = 2h/c$  [27]-[29], where  $h$  is the height of the vertical conductor and  $c$  is the velocity of light. That's why the maximum potential of the vertical conductor will occur at time  $t = 2h/c$ .

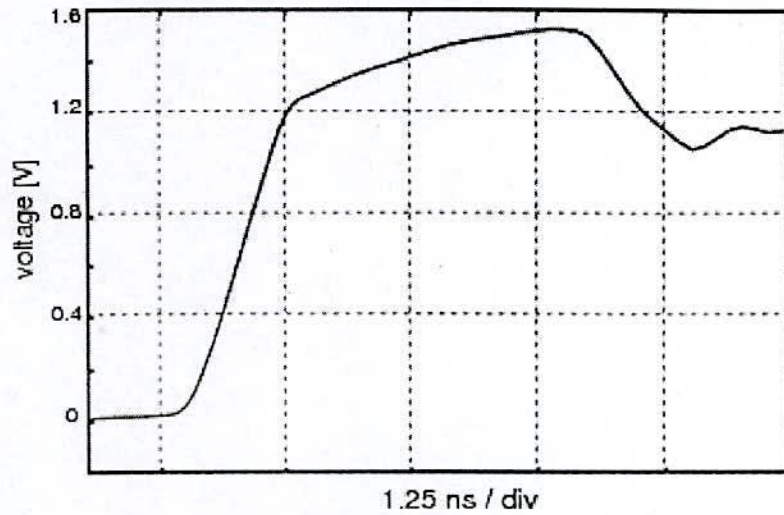
## 2.8 Surge Simulation by NEC-2

### 2.8.1 With Ground Plane

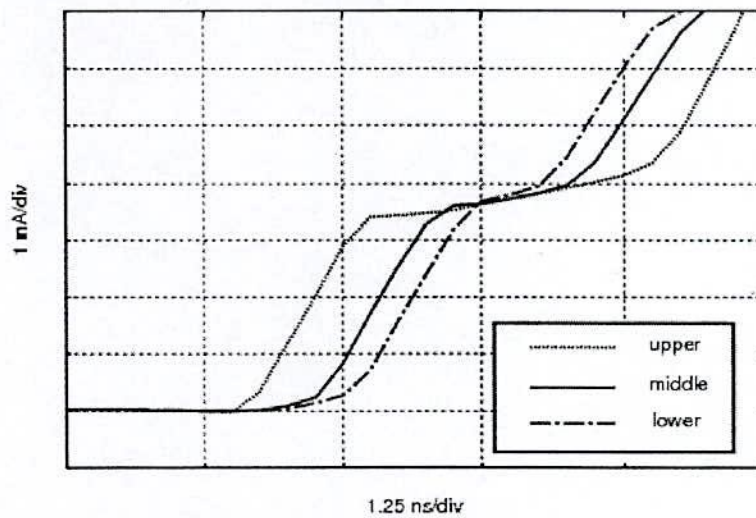
Considering the Fig. 2.3, we want to find the voltages and currents with the simulation by the NEC-2. Fig. 2.7 shows the simulation results by the NEC-2 of the voltage at the tower top and current through the vertical conductor respectively in case with ground plane. As soon as the reflected wave from the ground reaches the top of the conductor, the potential waveforms decrease, which is observed after  $t = 2h/c = 4$  ns that means the traveling wave is propagating at the velocity of light. The simulation result of voltage waveform at the tower top obtained is shown in Fig. 2.7 (a). The computed waveforms of current flowing through the vertical conductor are obtained at the location marked 'CT' in Fig. 2.3. The current sensors are placed about 20 cm apart in the vertical conductor to obtain the lower, middle and upper currents. These simulation results of currents waveforms obtained are given in Fig. 2.7 (b). The influence of ground plane can be observed in Fig. 2.7 (b), where the field produced by the current injected horizontally induce current of small magnitude before the actual surge current flowing through the vertical conductor. [21][22]. The simulation results are in well agreement with the FDTD results. [23].

### 2.8.2 Without Ground Plane

Fig. 2.8 shows the results of the voltage across the voltage measuring wire and currents through upper, middle and lower ends of the vertical conductor respectively in the absence of ground plane. However, in this of analysis, the waveforms of current through the vertical conductor are somewhat different from Fig. 2.7 (b). The major difference can be noticed at the starting zone of the lower end current and then current after rising to its peak. The surge currents through the vertical conductor after 1 ns of rise-time are almost flat and there is no such contribution of small induce current like Fig. 2.7 (b), because of absence of the ground plane for injected current. Also, the current starts flowing instantly through the vertical conductor without being delayed. The voltage waveforms reach their peaks after 4 ns, which indicates that a traveling wave propagates along the conductor with the velocity of light.

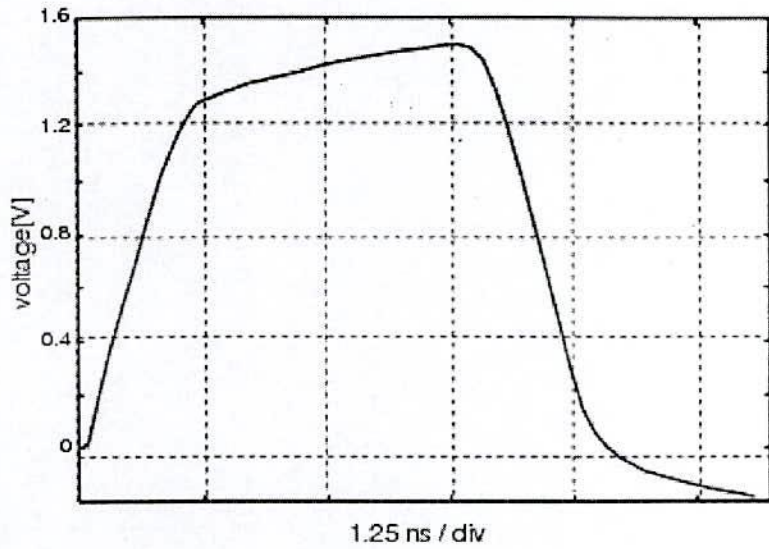


(a) Computed voltage waveform

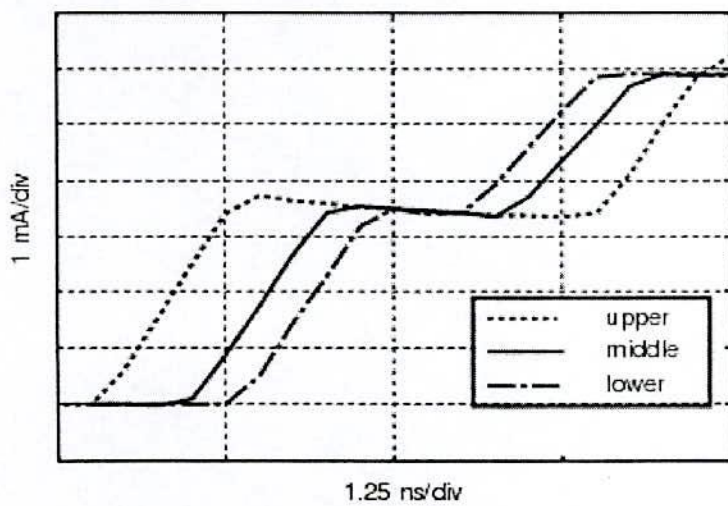


(b) Computed current waveform

Figure 2.7: NEC-2 results of voltage at the top and currents through the vertical conductor of 60 cm in case with ground plane.



(a) Computed voltage waveform



(b) Computed current waveforms

Figure 2.8: NEC-2 results of voltage at the top and currents through the vertical conductor of 60 cm in case without ground plane.



### 2.8.3 Surge Impedance

We define the surge impedance by the ratio of the instantaneous values of the voltage at the tower top or vertical conductor to the current flowing through it at the moment of voltage peak. The theoretical values of surge impedance with ground plane derived by Takahashi are just after the surge electric current reaches the ground and produced reflected current wave. There is another empirical formula of surge impedance equation (2.23), which is very close to equation (2.24). Here we plotted the empirical values of surge impedance along with the computed values considering the effect of ground plane and without ground

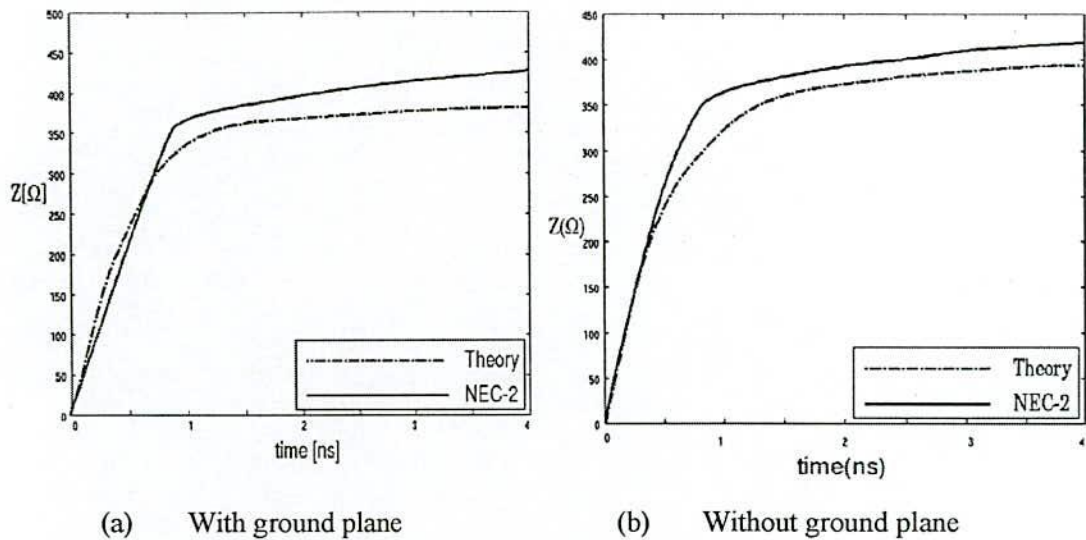


Figure 2.9: Surge impedance of the vertical conductor of 60 cm at  $0 < t \leq 2h/c$ .

plane along with the simulation at  $0 < t < 2h/c$ . Also we need to know surge impedance at  $t = 2h/c = 4$  ns. Computed values that are obtained by NEC-2 are approaching closely at  $t \approx 2h/c$ .

For comparison similar to the 60 cm of height model, 90 cm and 120 cm of height model was analyzed by the same procedure as described in the preceding sections. The injected current waveform was same in all these cases as shown in Fig. 2.5, in which the rise time was 1 ns. The voltage, current and impedance waveforms were obtained in these cases as shown in following Figs. 2.10, 2.11 and 2.12 respectively. In case of 90 cm model the current wave which is reflected from the ground reaches at the top after about 6 ns which shows that the electromagnetic wave propagates through the conductor with the velocity of

light. On the other hand, for 120 cm model the reflection occurs after 8 ns, which also shows that the propagation velocity is the velocity of light.

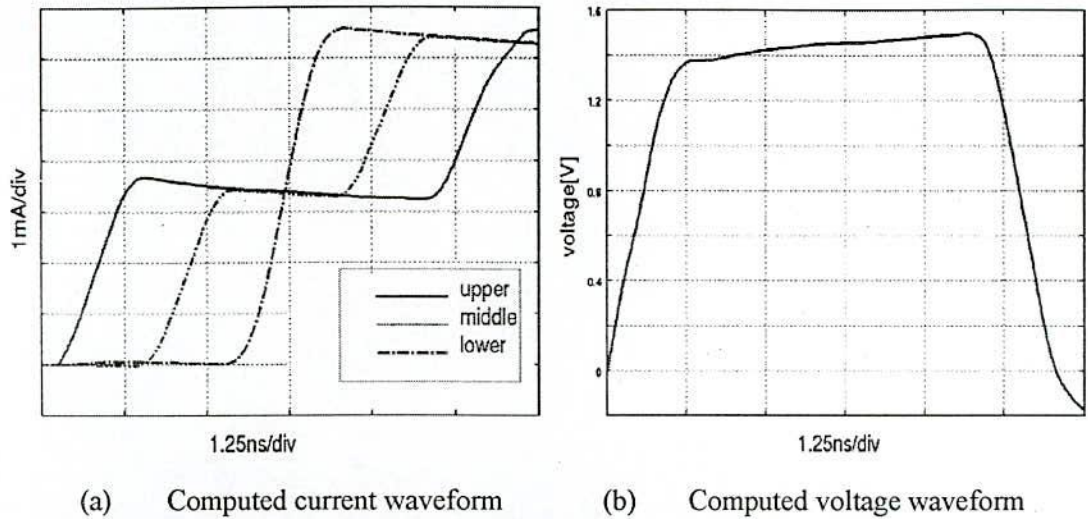


Figure 2.10: NEC-2 results of voltage at the top and currents through the vertical conductor of 90 cm in case without ground plane.

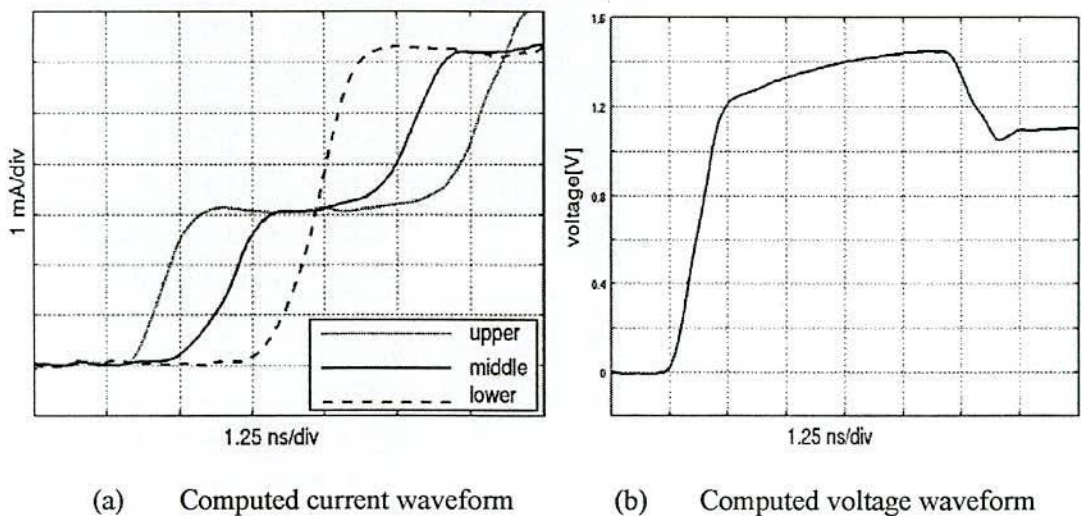
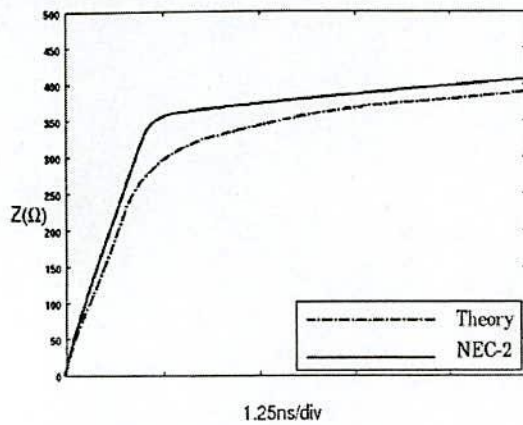
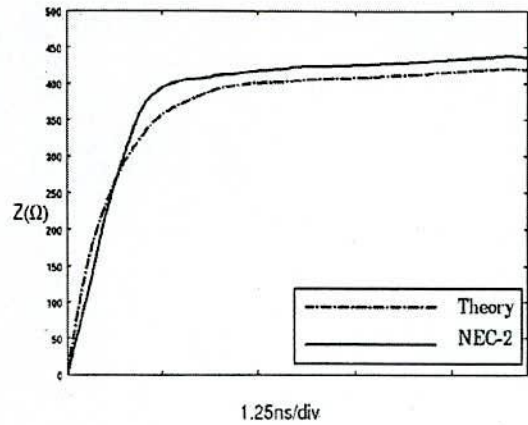


Figure 2.11: NEC-2 results of voltage at the top and currents through the vertical conductor of 90 cm in case with ground plane.

From the voltage and current the impedance curve is plotted as shown in Fig. 2.12. It is seen that value of surge impedance without ground plane case is more than with ground plane cases which was also in case of 60 cm model. The theoretical value of surge impedance can be explained by the theoretical value of Takahashi formula, which is considered without ground plane case and empirical formula of Hara *et al.* is considered with ground plane case.

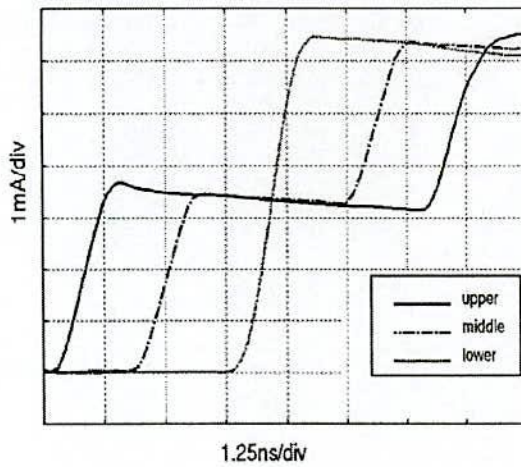


(a) With ground plane

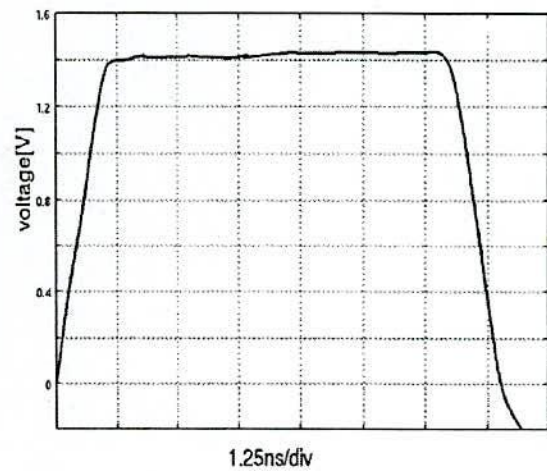


(b) Without ground plane

Figure 2.12: Surge impedance of the vertical conductor of 90 cm at  $0 < t \leq 2h/c$ .



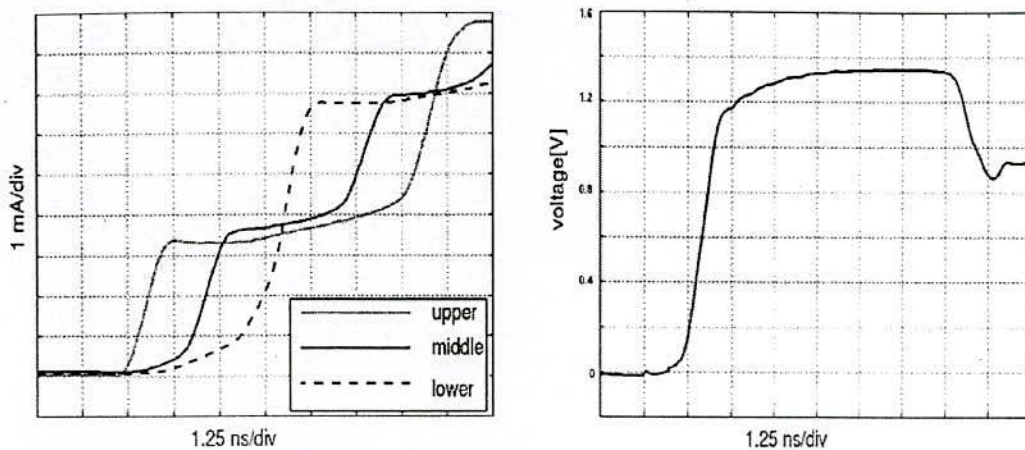
(a) Computed current waveform



(b) Computed voltage waveform

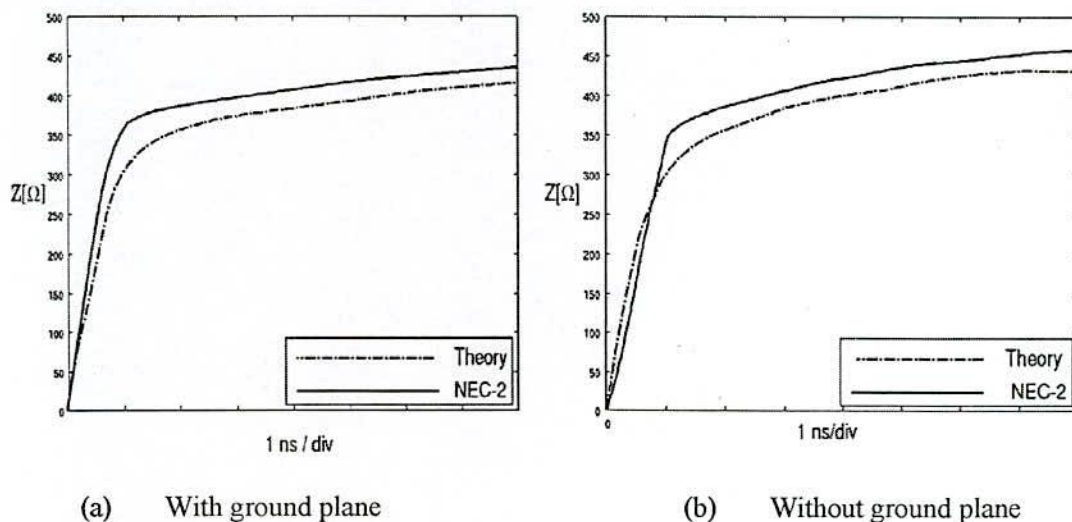
Figure 2.13: NEC-2 results of voltage at the top and currents through the vertical conductor of 120 cm in case without ground plane.





(a) Computed current waveform (b) Computed voltage waveform

Figure 2.14: NEC-2 results of voltage at the top and currents through the vertical conductor of 120 cm in case with ground plane.



(a) With ground plane (b) Without ground plane

Figure 2.15: Surge impedance of the vertical conductor of 120 cm at  $0 < t \leq 2h/c$ .

Similar to the 90 cm model, in case of 120 cm model we see that in both the cases the voltage waveform reaches their peak value after about 8 ns and then decreases. In case of the current wave, the reflection arrives after 8 ns, which shows that in this case electromagnetic wave also propagates with the velocity of light. The value of surge impedance without ground plane case is more than in case with ground plane as explained in 60 cm model. It is seen that the value of surge impedance increases with the time as long as it reaches to the surge impedance value of the vertical conductor and then decreases.

### 2.8.4 Influence of the Method of Current Injection

For the analysis of current injection at the different point is numerically simulated. In this case a pulse generator is inserted into the current lead wire at different places from the top of the vertical conductor in the current lead wire as shown in Fig. 2.16. The pulse generator is placed as in case (i) at 150 cm above, (ii) at 100 cm above the top of the vertical conductor and (iii) also at the top of the vertical conductor. These three arrangements of pulse generator are simulated with the help of NEC-2. The computed waveforms of the conductor top voltages and currents

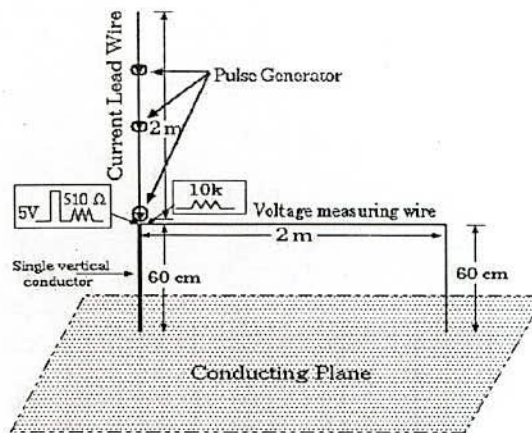


Figure 2.16: Arrangement for the analysis by the direct method, where a pulse generator is placed at different position in the current lead wire.

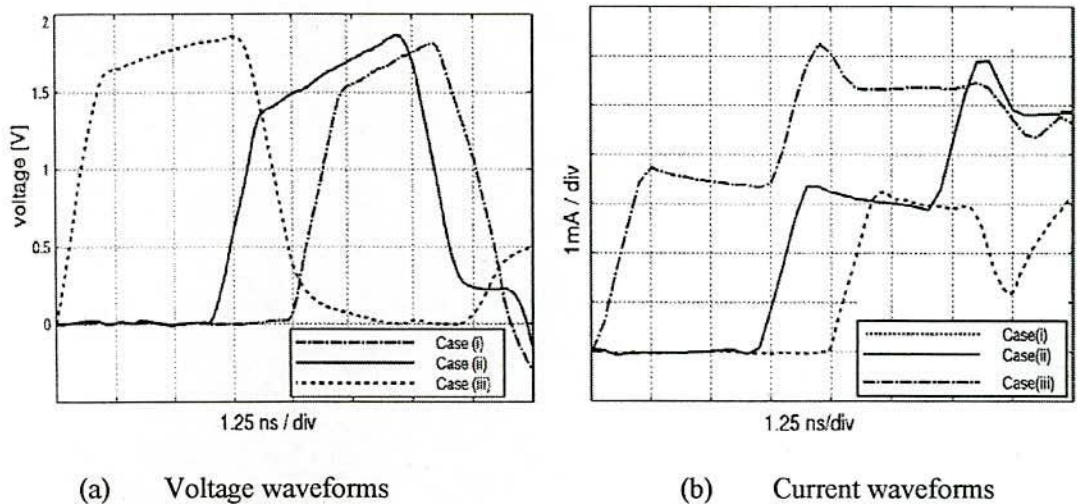


Figure 2.17: Computed waveforms of voltage and currents for injection at different height of the current lead wire.

flowing into the conductor are shown in Fig. 2.17. The broken line, solid line and chain lines results correspond to case (i), case (ii) and case (iii) respectively. The voltage waveform for case (iii) reaches its peak value at  $t = 2h/c = 4$  ns which shows that the propagation velocity is same as light. On the other hand for other two cases there is a time delay of 3.4 ns in case (ii) and 5 ns in case (i), which also show that the electromagnetic wave is propagating through the conductor with the velocity of light. For the current waveforms it is observed that only in case (iii) the reflection from the perfectly conducting ground occurs after 4 ns. But in other two cases there are time delays for reflection due to time required to propagate electromagnetic wave through the vertical conductor.

### 2.8.5 Effect of Changing Segment Length

The main electrical consideration is segment length  $\Delta L$  relative to the wavelength  $\lambda$ . Generally,  $\Delta L$  should be less than about  $0.1\lambda$  at the desired frequency. Somewhat longer segments may be acceptable on long wires with no abrupt changes while shorter segments,  $0.05\lambda$  or less, may be needed in modeling critical regions of an antenna. The size of the segments determines the resolution in solving for the current on the model since the current is computed at the center of each segment. Extremely short segments, less than about  $10^{-3}\lambda$ , should also be avoided since the similarity of the constant and cosine components of the current expansion leads to numerical inaccuracy. So the vertical conductor model of height 90 cm was taken into account for analysis by changing segments length according to the modeling guidelines. Here for simulation with NEC-2 the segment size was taken as 5 cm, 10

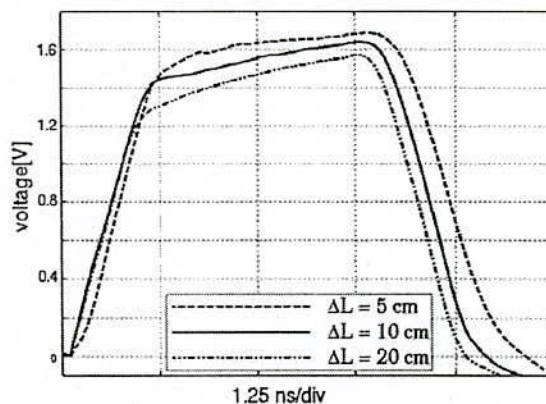


Figure 2.18: Voltage at the tower top in case of changing segment length.





cm and 20 cm in length. The output waveforms of tower top voltage were obtained are almost similar to the Fig. 2.10 (b) means it is acceptable within the accuracy maintain in the analysis. So , within the modeling limit the segment length should be as small as possible to obtain the better result, also to maintain the accuracy although if the segment length decreases the computation time increases.

### 2.8.6 Effect of Changing Radius and Height

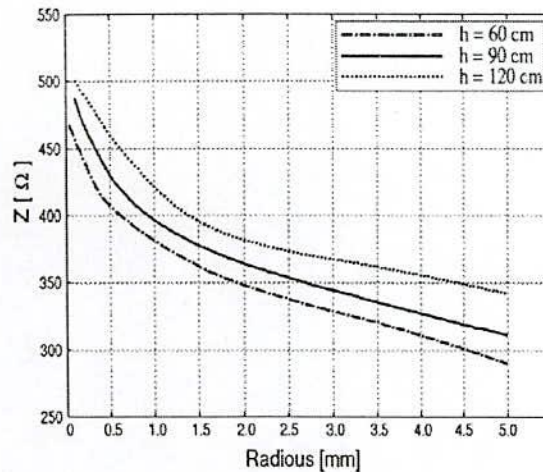


Figure 2.19: Waveforms by varying radius and height of the conductor.

For the numerical analysis with NEC-2, the entire structure needs to be modeled by combination of cylindrical segments that must be short enough compared to the wavelength of interest. The accuracy of result of NEC-2 by varying the radius of the considered reduced scale vertical conductor model over perfectly conducting ground is investigated here by simulation approach. In the current analysis the height of the vertical conductor is set to 60 cm and being considered it as a cylinder the radius of the conductor is varied from 0.05 mm to 5 mm for observation. A step current pulse generator having pulse voltage of 5 V in magnitude, risetime of 1 ns and pulse width of 40 ns was taken for the analysis. Here the segment length  $\Delta L = 10$  cm was taken which must satisfy the condition that radius should be smaller than  $\Delta L / 8$ . Computation is carried out in time range of 0.25 ns with stepping frequency of 7.8125 MHz. The voltage at the top of the vertical conductor was taken and current was computed. Then from the computed value of voltage and current the surge impedance as defined by the ratio of the instantaneous values of the voltage at the tower top of vertical conductor to the current flowing through it at the moment of voltage peak is

determined. The value of surge impedance can also be determined by the theoretical formula which is very close to the well-known empirical formula given as in case of with ground plane. Similarly, 90 cm of height and 120 cm of height vertical conductors were considered and the data was taken. By plotting the simulation result, the effects of varying radius and height on the surge impedance are shown in Fig. 2.19.

From the graph it is seen that if the radius of the vertical conductor is increased then the value of surge impedance decreases. It was also noticeable that with the increase of the length of the vertical conductor the value of surge impedance increases. Thus it can be shown that the accuracy is satisfactory when a model comprises segments with a uniform radius smaller than about  $\Delta L / 8$ .

Although, the simulation was carried out for the arrangement with ground plane, however the other model also gives the same results.

### 2.8.7 Computation Time

For the case of NEC-2, computation is carried out in the frequency range of 7.813 MHz to 4 GHz with the increment step of 7.813 MHz. This corresponds to the time range of 0 to 128 ns with 0.25 ns increments. The computation time for the output of NEC-2 block of the flow chart of Fig. 2.6, with Intel Celeron 700 MHz processor with 128 MB RAM is about 56 seconds with the ground plane case and 30 seconds without ground plane case for 60 cm model. For 90 cm model, 60 seconds with the ground plane case and 35 seconds without ground plane case and for 120 cm model, 70 seconds with the ground plane case and 40 seconds without ground plane case are observed.

## 2.9 Summary

The difference of the surge impedances depends on the arrangement in the current lead wire, which can be explained by the electric field associated with the steep-front currents flowing in the current lead wire, the voltage measuring wire or earth wire and the vertical conductor or tower. With vertically applied input or without ground plane case, the positive surge current from the pulse generator flowing into the vertical conductor and the negative current propagating up the vertical current lead wire produce the strong upward electric field. This makes the injected current split more into the voltage measuring wire and less into the



vertical conductor than in the case of Fig. 2.7 (b), resulting in higher vertical conductor surge impedances.

On the other hand, a strong horizontal electric field is produced by the negative current into the horizontal current lead wire. This makes the injected current split more into the vertical conductor and less into the voltage measuring wire than in the case of Fig. 2.8 (b),

Table 2.1: Surge impedance comparison table:

	60 cm			90 cm			120 cm		
	Without ground plane ( $\Omega$ )	With ground plane ( $\Omega$ )	Effect of ground plane in %	Without ground plane ( $\Omega$ )	With ground plane ( $\Omega$ )	Effect of ground plane in %	Without ground plane ( $\Omega$ )	With ground plane ( $\Omega$ )	Effect of ground plane in %
Theory	395	368	6.8	420	393	6.4	436	410	6
NEC-2	425	395	7	440	402	8.6	460	415	9.7

which results in lower surge impedances as shown in Fig. 2.9 also demonstrates in Table 2.1. The effect of ground plane can also be observed from the Table 2.1.

It was also observed for 90 cm and 120 cm models, which has been shown in Fig. 2.10 to 2.15. It must be noticeable that as the height of the vertical conductor with same radius was increasing the value of surge impedance was increasing as it is found according to the theoretical formula. The maximum difference between the theoretical and computed values is found to be about 7.6 % in case without ground plane and 7.35 % in case with ground plane. The maximum effect of ground plane is also observed to be less than 10 % with the simulation and theoretical investigation [27]-[30].



# Chapter 3

## Surge Analysis of Four Parallel Conductors

### 3.1 Introduction

In the preceding chapter the lightning surge characteristics are simulated and analyzed for reduced scale model of single vertical conductor. It should be noted that lightning is responsible for severe electromagnetic stress in electric and electronic systems that frequently result in damages or operational outages. The evaluation of such a stress is very important for lightning protection. So in this chapter lightning surge response for four parallel conductors model has been taken into account. The surge impedance obtained from four parallel conductors is details analyzed in this chapter for both cases, i.e., with ground and without ground as it was for single vertical conductor.

Fig. 3.1 shows the structures subjected to analysis. The single vertical conductor as shown in Fig. 3.1 (a) has a radius of 5 mm where as the vertical four conductors in Fig. 3.1 (b) has a radius of 16.5 mm and 404 mm apart. A steep-front current having a rise time of 5 ns was injected into a current lead wire as shown in Fig. 3.2. In Fig. 3.2 the injected ramp also compared with the computed current at the input terminal. Ffor the numerical analysis, the conductor system needs to be modeled with segments according to the modeling guidelines stated in the preceding chapter. It is not difficult to satisfy recommended conditions except the following one:  $0.001 \lambda \leq \Delta L \leq 0.1 \lambda$ . This requirement is too severe to be satisfied exactly,

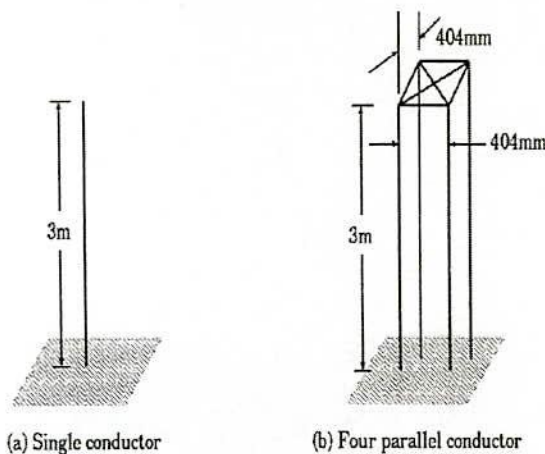


Figure 3.1: Structure subjected to analysis.

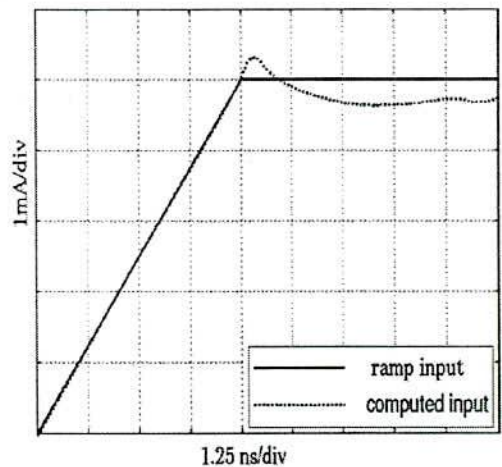


Figure 3.2 Comparison of injected and computed input waveforms for analysis .

since the wider frequency range is needed here to investigate the transient characteristics of such a system. However the author found the following condition yielding reasonable computation results by trial and error process.

Frequency range: 1.5625 MHz to 0.8000 GHz with 1.5625 MHz increment step and  
 Segment length: 0.202 m to 0.300 m.

The above frequency range corresponds to the time range of 0 to 640 ns with 1.25 ns increments.

### 3.2 With Ground Plane

The following Fig.3.3 shows the arrangement of the four parallel conductors model to be analyzed with ground plane case. To evaluate the voltage of the top of a structure, 10 k $\Omega$  resis-

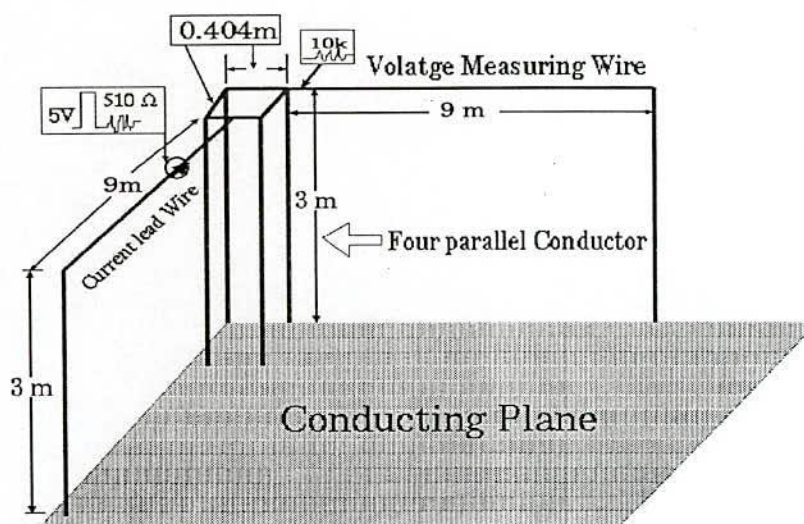
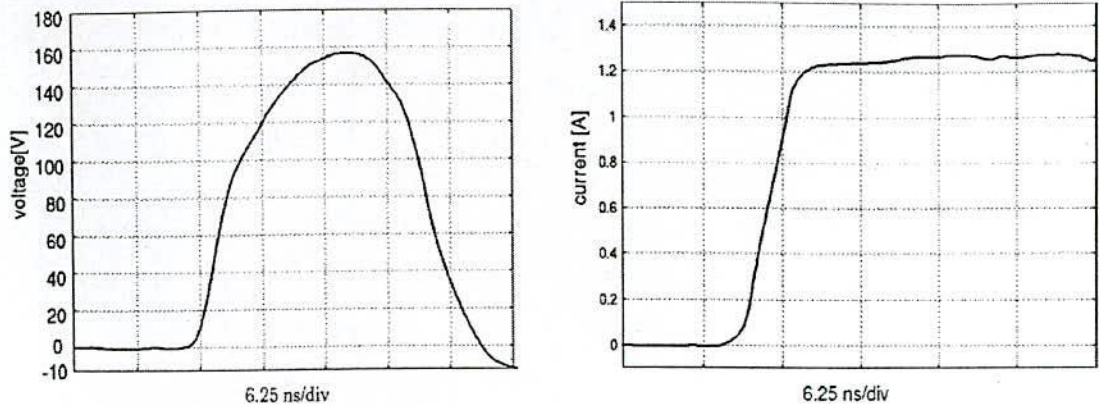


Figure 3.3: Arrangement of four parallel conductor system for simulation using NEC-2 with ground plane.

tance was inserted between the top of a structure and the end of the voltage measuring wire and the waveform of the current flowing through the resistance was calculated. The system of structures under the numerical analysis was postulated to be on the perfectly conducting ground. This postulation is used throughout in this thesis. Fig. 3.4 shows the computed waveforms of the tower top voltage and the current at the top of the four parallel conductors.

If a travelling wave propagates along the tower at the velocity of light the reflected wave from the ground should return to the tower top after the round-trip time of a travelling wave in the tower which is 20 ns for this structure in Fig. 3.3. But from the computed result it is seen that





(a) Computed voltage (b) Computed current

Figure 3.4 NEC-2 results of voltage at the top and current waveforms for the four parallel conductors with ground plane case.

voltage waveforms reach their peaks about 17 ns after the beginning which indicate that a negative voltage wave arrives at the top before the arrival of the reflected wave from the ground. This phenomenon is due to the electromagnetic field of TEM mode illuminating the structure, i.e., the electromagnetic wave associated with a travelling wave in the current lead wire arrives at the structure foot simultaneously with the arrival at the top of a structure and a negative voltage wave is induced at the structure foot before the occurrence of the reflection of the travelling wave propagating down from the top of the structure. This induced wave is observed in the current waveform as in Fig. 3.4 (b).

The analysis was carried out for different rise time as shown in Fig. 3.5, which were 5 ns and 2.5 ns respectively. From the output it is seen that for small rise time the voltage of the structure at the top reaches the peak value earlier than the other.

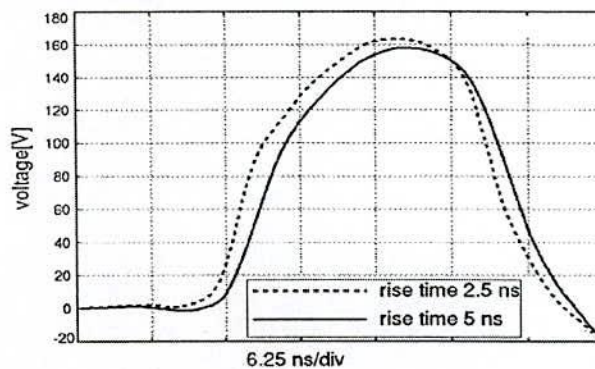
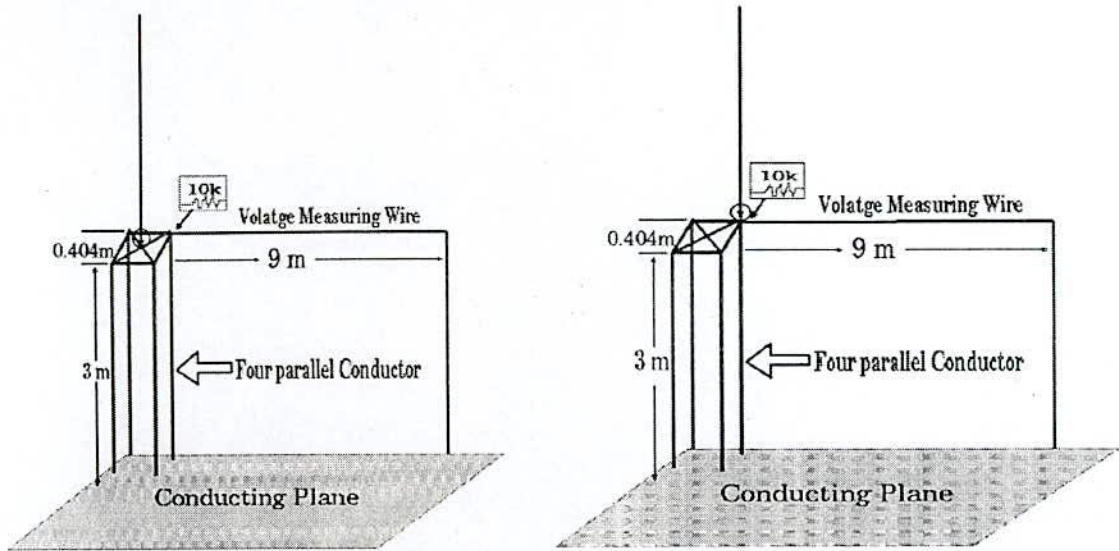


Figure 3.5: NEC-2 results of voltage waveforms at the top of the four parallel conductors with ground plane case for different rise time.



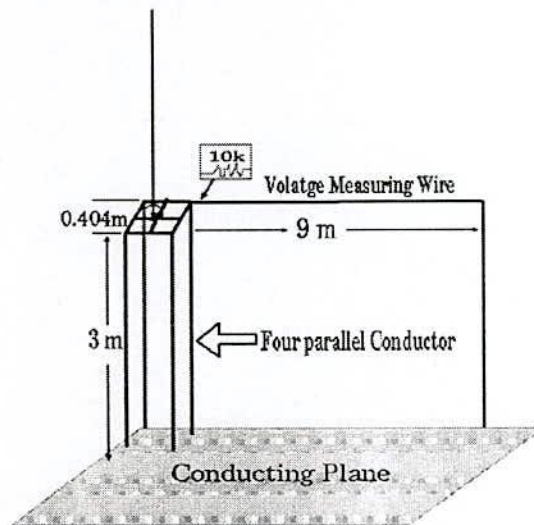
### 3.3 Without Ground Plane

The following Figs. 3.6 (a), (b) and (c) show the arrangement of the four parallel conductors model to be analyzed without ground plane cases.



(a) Injection is at the center top of cross configuration

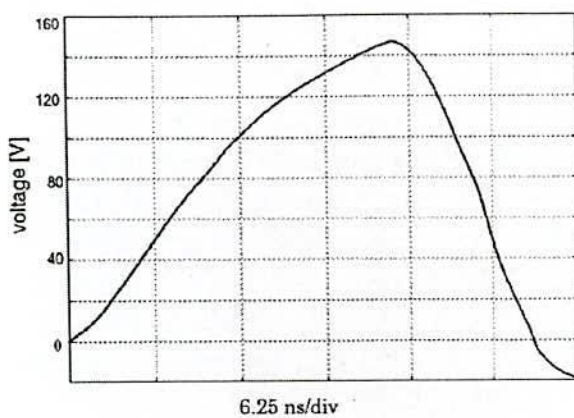
(b) Injection is at one end of top of cross configuration



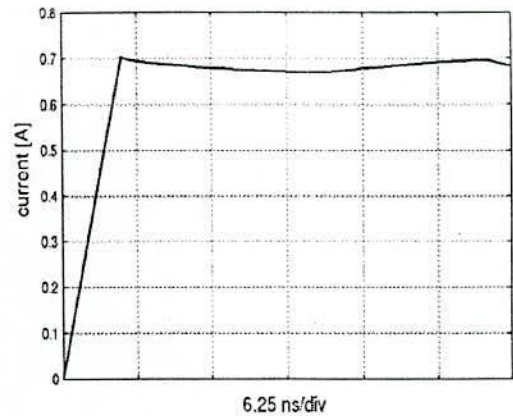
(c) Injection is at the junction of plus configuration

Figure 3.6: Arrangement of four parallel conductors system for simulation in case without ground plane.

On the other hand, from numerical analysis by NEC-2 the computed waveforms of the voltage and the current at the top of the four parallel conductors are obtained as shown in Figs. 3.7, 3.8 and 3.9. The rise time was set to be 5 ns as shown in the following Figs. In Fig. 3.7 and 3.8 the voltage waveform rises exponentially and reaches their peak after 21 ns, which shows that in this case the electromagnetic wave propagates along the conductor with the velocity of light. Then it decreases downward as the reflection comes from the ground. But in Fig. 3.9 the voltage waveform rises abnormally and reaches its peak after 25 ns, which is not similar to the other cases.

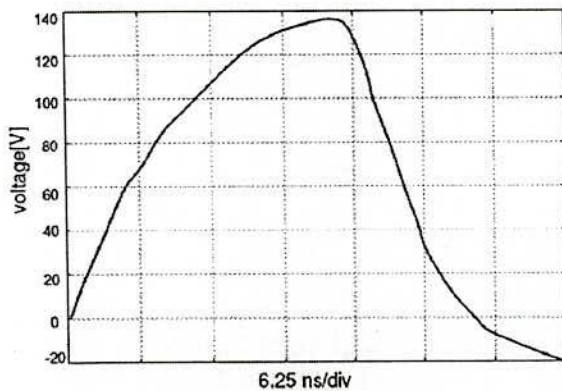


(a) Voltage waveform

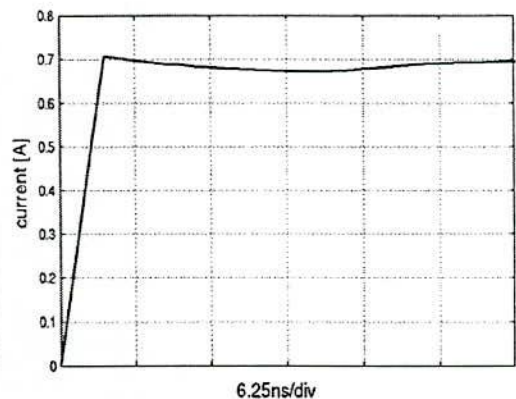


(b) Current waveform

Figure 3.7: Computed waveforms of the voltage and the current at the top for Fig. 3.6(a).

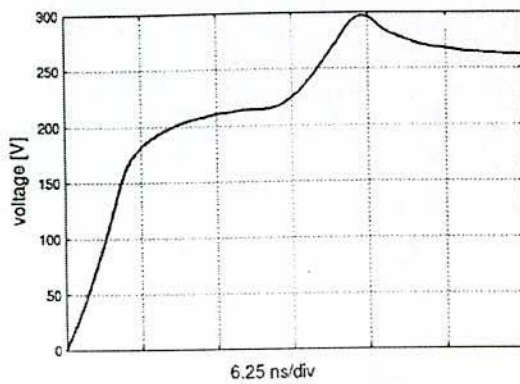


(a) Voltage waveform

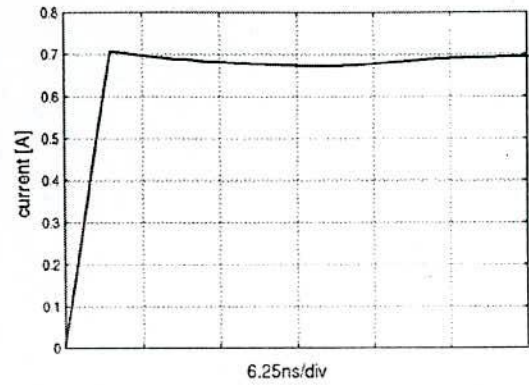


(b) Current waveform

Figure. 3.8: Computed waveforms of the voltage and the current at the top for Fig. 3.6(b).



a) Voltage waveform



(b) Current waveform

Figure 3.9: Computed waveforms of the voltage and the current at the top for Fig. 3.6(c).

As the output for structure of Figs. 3.6 (a) and (b) show the characteristics like single vertical conductor so this structure is suitable for analysis and design. On the other hand, structure of Fig. 3.6 (c) is not suitable for design purposes.

### 3.4 Surge Impedances

Then the tower surge impedances are calculated where the tower surge impedance is defined as the ratio of the instantaneous values of the voltage to the current at the moment of voltage peak [28]-[30]. The computed tower surge impedances are summarized in table 3.1:

Table 3.1: Simulation results of surge impedance

Configuration for NEC-2	With ground ( $\Omega$ )	Without ground ( $\Omega$ )
For Figure 3.3 and 3.6 (a)	126	195
For Figure 3.3 and 3.6 (b)	126	205
For Figure 3.3 and 3.6 (c)	126	414

### 3.5 Computation time:

The computation time for the output of NEC-2 block of the flow chart of Fig. 2.6, with a Pentium II 300 MHz processor with 128 MB RAM for the analysis is within 90 seconds. The input data to NEC-2 are shown in Appendix C.



### 3.6 Summary

These results can be used to estimate the tower surge impedance of the standard arrangement with a vertical current lead wire and horizontal voltage measuring wire as well as with ground plane in case of four parallel vertical conductor models. From the analysis Figs. 3.6 (a) and 3.6 (b) as the models are recommended. This analysis will help us to configure the structure of control building and high tech building when highly sophisticated instruments and electronic equipments are installed.

## Chapter 4

### Lightning Surge Response on Actual Tower

#### 4.1 Introduction:

Lightning performance of transmission lines is an important issue of major interest for electric utility companies. Now a days, with the increasing requirement for power quality, this matter has been deserving even more attention. In the previous research reduced scale has been taken into account for analysis. It is better for understanding and also for simulation. But usually in real life actual tower subjected to lightning. So, it is needed to analysis the characteristics of actual tower when subjected to lightning as reduced scale model tower. That is why the author simulates an actual tower to obtain the surge characteristics phenomena. In this case the three-phase conductor and earth wire have been taken into analysis. The apparent characteristics of a tower may be influenced by the presence of an earth wire. However this issue has been paid little attention in the modeling of a tower for the NEC-2 simulations. In this chapter, the surge characteristics of an earth-wired tower as well as phase conductors of the tower struck by lightning are studied with the help of NEC-2 in case of direct and indirect stroke. Particularly, this chapter present some results like the tower surge impedance, tower footing impedance and the voltage and current of the earth wire and phase conductors concerning the computational simulation of electromagnetic transients in transmission lines caused by direct and indirect strikes of lightning.

#### 4.2 Numerical Electromagnetic Analysis of Earth-Wired Tower Struck by Lightning

In this type of simulation, two kinds of lightning stroke as indicated in the previous chapter are simulated: one is a return stroke and other is a downward travelling current waveform as shown in Fig. 4.1. In the case of a return stroke to a tower, a downward leader, which is similar to a charged vertical transmission line whose lower end is open, contacts the top of the tower. This situation can be simulated by placing a pulse current generator at the tower top, except for an actually slower velocity of return current wave than the velocity of light. For reduced scale model which employed a spiral wire or a straight wire suspended vertically above the tower, showed that the speed of upward moving current produces only second-order effects

on the surge characteristics of a tower. Therefore the analysis employing a vertical straight wire as a current lead wire which can properly evaluate tower characteristics.

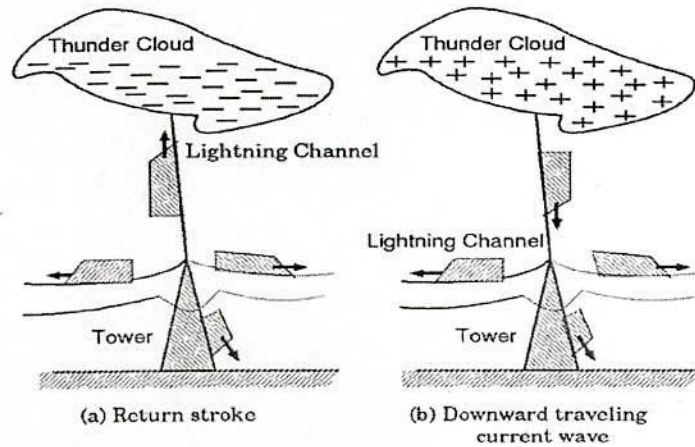


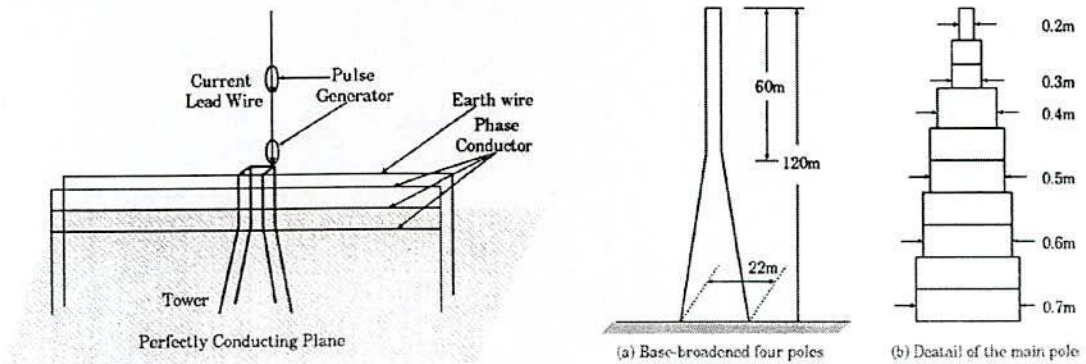
Figure 4.1: Schematic diagrams of different types of lightning strokes to the top of a tower.

On the other hand, many of the lightning strokes hitting towers on the coastal area of the Sea of Japan in winter begin with upward leaders from the towers [31], and many current pulse are not produced by what are called return strokes [32]. In such kind of strokes, a current wave is thought to propagate down the lightning channel from the cloud to the tower top. For the simulation of this situation, a pulse current generator needs to be remotely placed above the channel. In the present analysis, a pulse current generator is inserted into the current lead wire at 240 m from the tower top, where the current lead wire is 480 m in length.

The arrangement for the analysis is shown in Fig. 4.2. The model tower shown in Fig. 4.2, is composed of four main poles. The ground plane was considered perfectly conducting plane of Copper with conductivity  $5.8 \times 10^7$  mho/meter. Each pole is connected to the perfectly conducting plane through  $40 \Omega$  resistance to realize the tower footing resistance of  $10 \Omega$ . The impedance seen by a lightning surge flowing from the tower base to true ground. The risk for backflashover increases with increasing footing impedance. Backflashover occurs when lightning strikes the tower structure or overhead shield wires. The lightning discharge current, flowing through the tower and tower footing impedance, produces potential differences across the line insulation. If the line insulation strength is exceeded flashover occurs i.e. a backflashover. Backflashover is most prevalent when tower footing impedance is high. So, low value of tower footing impedance is desirable in order to avoid backflashover. Compact lines;



transmission lines with reduced clearances between phases and between phase and earth and with lower insulation level withstand than for normal lines for the same system voltage.



(a) Arrangement of tower for simulation

(b) Details of the tower

Figure 4.2: The structure of the model tower subjected to analysis.

A horizontal earth wire is attached to the tower top at a height of 120 m and phase conductors are stretched at a height of 108 m, 84 m and 60 m respectively, at a distance of 10m from the tower body. Each conductor or wire is 960 m in length and 0.1 m in radius. The ends of them are stretched down and connected to the ground through matching resistance. This terminating condition does not affect the phenomena within  $3.2 \mu\text{sec}$ . An insulator voltage is evaluated through the current flowing a  $100 \text{ k}\Omega$  resistive element inserted between the tower body and the phase conductor. To save the computation time, the phase conductor of interest can only be considered, and other phase conductors are removed.

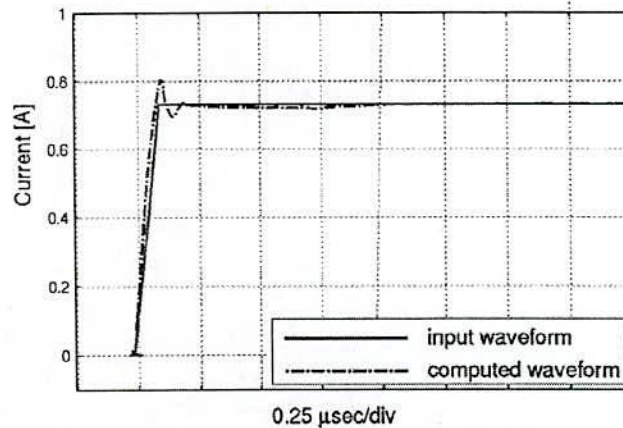


Figure 4.3: Comparison of input and computed current waveform.

Similar to the reduced scale model and four parallel models this actual tower model is analyzed for both cases such as with and without ground plane cases. A sample input data deck to NEC-2 for the analysis is shown in Appendix D. The injected and computed waveforms have been shown in Fig. 4.3.

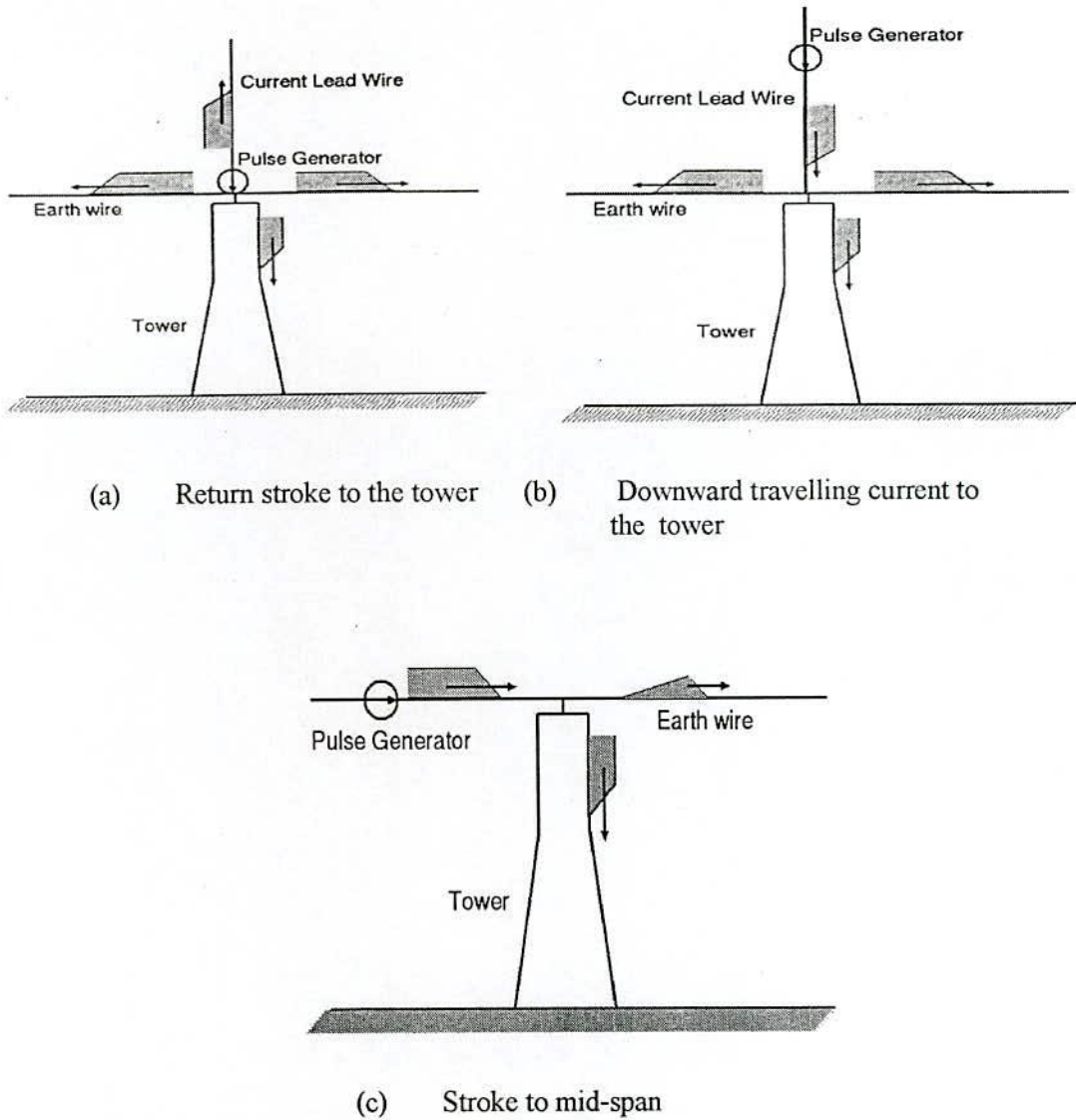


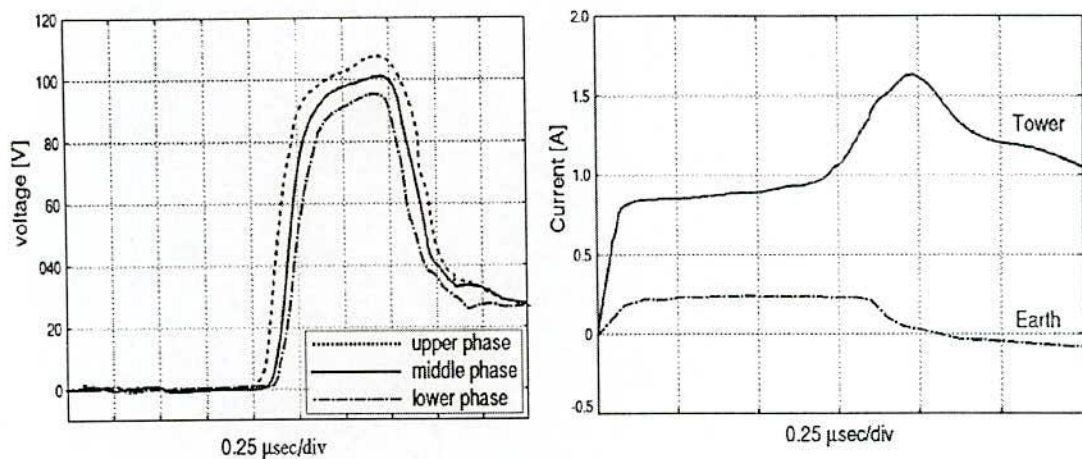
Figure 4.4 Schematic diagram for simulation of current splitting ratio between a tower and earth wire.

Fig. 4.4 illustrates schematic diagram to simulate current splitting ratio between the tower and earth wire. Fig. 4.4 (a) simulates a lightning return stroke to the tower that is called direct stroke or without ground plane, Fig. 4.4 (b) does a downward travelling current to the

tower top and Fig. 4.4 (c) does a stroke to the mid-span. Simulation employing Fig. 4.4 (c) have been called the refraction or with ground plane case. In Fig. 4.4 (a) a pulse generator is placed on the tower top and is connected to a long vertical current lead wire, while in Fig. 4.4 (b), a pulse generator is inserted into the current lead wire at 150 m upward from the tower top. A long earth wire is stretched horizontally. In Fig. 4.4 (c), a pulse generator is inserted into the earth wire at 150 m left from the tower top.

### 4.3 With Ground Plane

Considering the Fig. 4.4 (c) the simulation was carried out by NEC-2. The output voltage at different phases of different height and current waveforms were obtained as shown in Fig. 4.5.



(a) Voltage at different phases

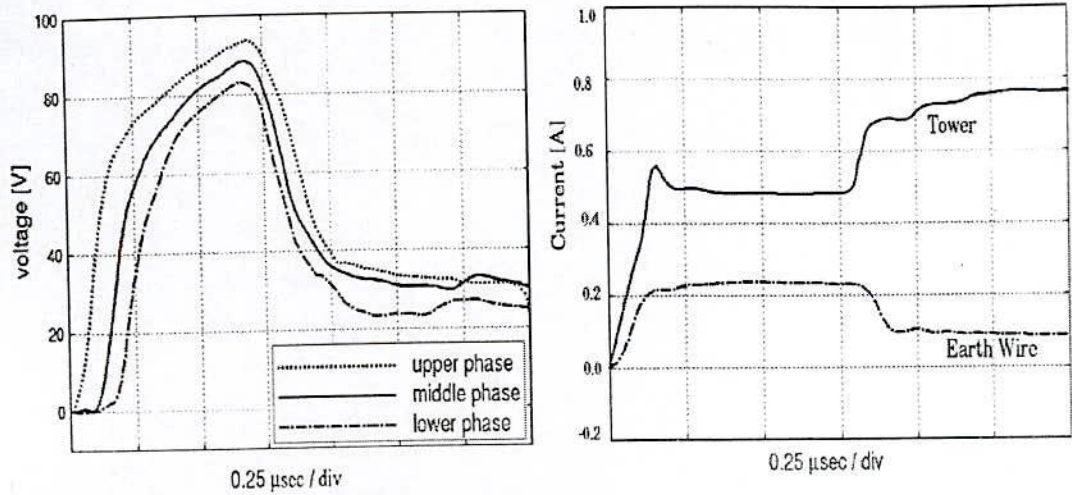
(b) Current in the tower and earth wire due to stroke to mid-span

Figure 4.5 Computed waveforms of insulator voltage and splitting current into the tower top in case of horizontal injection.

### 4.4 Without Ground Plane

The simulation was also carried out without ground plane case as shown in the arrangement in Fig. 4.4 (a). The computed waveforms of voltage and current splitting ratio into the tower and earth wire are shown in Fig. 4.6. The current splitting ratio into the tower and earth wire is also simulated in case of downward travelling current into the tower and computed waveform is shown in Fig. 4.7.





(a) Voltage at different phases (b) Current in the tower and earth wire due to return stroke to the tower

Figure 4.6 Computed waveforms of insulator voltage and splitting current into the tower top in case of vertical injection.

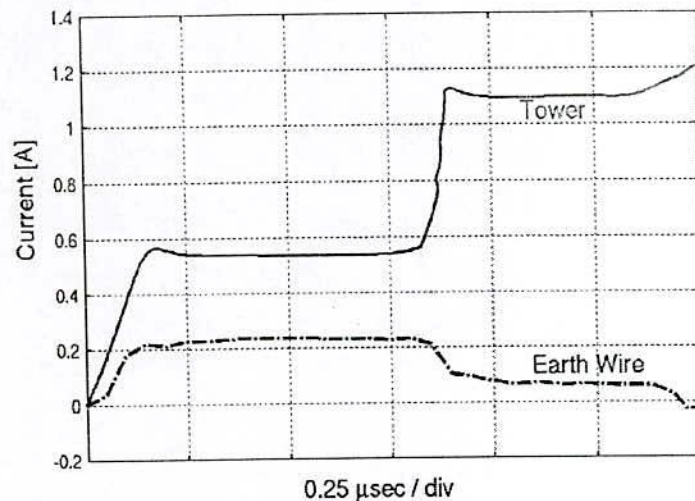


Figure 4.7 Computed waveforms of current splitting ratio into the tower and earth wire due to downward travelling current to the tower.

#### 4.5 Surge impedance :

From the above Figs. 4.5 and 4.6 for both with and without ground plane cases the tower surge impedances are evaluated at the moment of voltage peak and waveform of current into the tower top in case of vertical injection. In case of indirect stroke the current in the tower is more than direct stroke. The surge impedance are calculated and summarized in the table 4.1:

Table 4.1: Surge impedance of the actual tower model at  $t \approx 2h/c$

Arrangement	With ground ( $\Omega$ )			Without ground ( $\Omega$ )		
	Upper	Middle	Lower	Upper	Middle	lower
Surge impedance	135	125	107	205	190	170

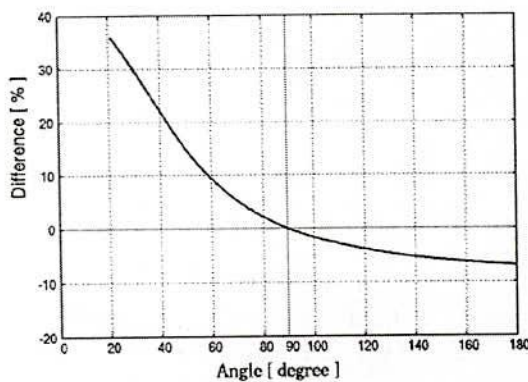
From the above it is seen that the surge impedance for the ground plane is naturally much lower than of without ground plane as it was ascertained in the preceding sections.

#### 4.6 Influence of the Arrangements of Current lead wire

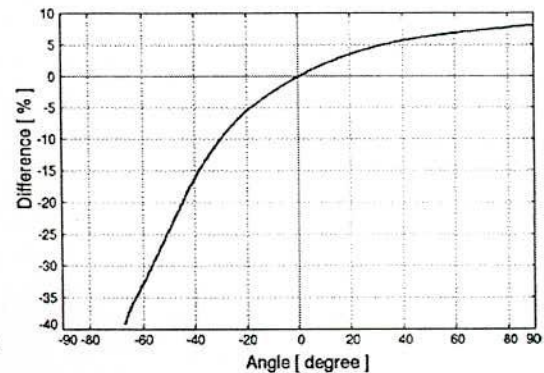
The analysis was carried out in different arrangement of the current lead wire as:

- (i) vertical,
- (ii) horizontal and perpendicular to a horizontal voltage measuring wire and
- (iii) horizontal and in extension of a voltage measuring wire .

Fig. 4.8 illustrates the effect of the arrangement of current lead wire on the tower surge impedance in details. For the numerical analysis the voltage measuring wire is stretched horizontally. In Fig. 4.8 (a) a current lead wire is in a horizontal plane at the height of the tower and the angle between the current lead wire and the voltage measuring wire is varied from  $30^\circ$  to  $180^\circ$  . The angle of  $90^\circ$  corresponds to the case (ii) and that of is taken  $180^\circ$  does the case (iii). In Fig. 4.8 (b) a current lead wire is in a plane perpendicular to the voltage measuring and the angle between the current lead wire and a horizontal plane at the height of the tower top is varied from  $-60^\circ$  to  $90^\circ$  . Negative sign of the angle shows that the current lead wire is stretched down to the earth. The angle of  $90^\circ$  corresponds to the case (i), and that of  $0^\circ$  does



(a) Effect of the angle between current lead wire and voltage measuring wire



(b) Effect of the angle between current lead wire and the tower

Figure. 4.8 Influence of the arrangement of the current lead wire.

the case (ii). In both cases tower surge impedance for the case (ii) is selected as the reference value.

After calculating the difference the curve of difference verses angle between current lead wire and voltage-measuring wire is plotted as shown in figure above. As the angle of injection increasing from  $30^\circ$  to  $180^\circ$  the surge impedance is decreasing continuously and the difference due to arrangement of the current lead wire becomes greater if the angle between the wires is less than  $90^\circ$ .

#### 4.7 Estimation of Surge Impedance of Double-Circuit Transmission Tower

Fig. 4.9 illustrates 1000 kV and 500 kV double-circuit transmission towers, which are typical lattice tower used in different countries. The surge impedance of these towers has been simulated by direct method. In this method the earth wires were disconnected. The tower of UHV I was simulated in the vertical arrangement on a 100-to-1 reduced scale model, and the surge impedance was  $200 \Omega$ . The others are full-sized towers and were simulated in different arrangements of current lead wire. The surge impedance of these towers for vertical arrangement are summarized in table 4.2, with the dimensions of the towers, with the measured value.

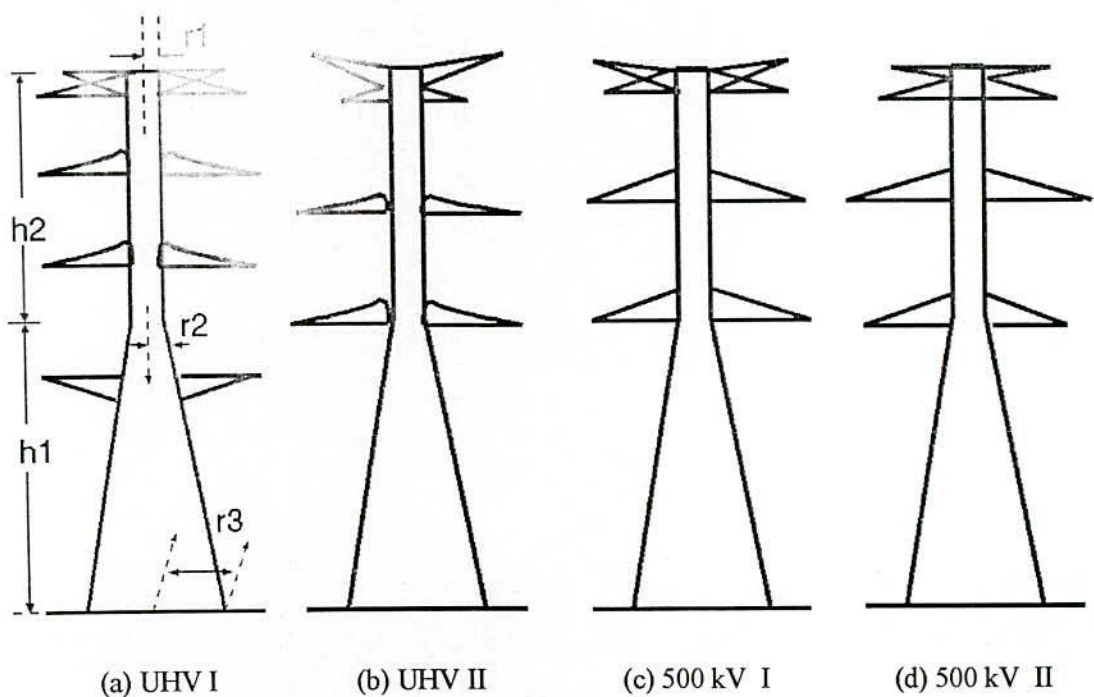


Figure 4.9 : Structures of 1000 kV and 500 kV double circuit towers.



Table 4.2: Surge impedance of various double-circuit towers simulated and measured by direct method and dimension of them:

Tower	UHV I [36]	UHV II [11]	500 kV I [9]	500 kV II [10]
$Z_T (\Omega)$ Measured	144	145	148	145
$Z_T (\Omega)$ Simulated	200	195	205	190
$r_1$ (m)	3.0	2.5	1.5	1.0
$r_2$ (m)	6.5	4.0	2.3	1.9
$r_3$ (m)	14	11	5.6	4.0
$h_1$ (m)	80	60	31	24
$h_2$ (m)	80	60	31	24

The dimensions of UHV tower indicated that in table 4.2 are those of the original full-sized tower. Here the correction was made by using Fig. 4.8. In the case of UHV II tower, for example, the current lead wire and the voltage measuring wire on a horizontal plane in the angle of  $130^\circ$ , it is known from Fig. 4.8 (a) that the surge impedance of  $165 \Omega$  would be  $175 \Omega$  if the angle between the two wires were  $90^\circ$ . This value of  $175 \Omega$  corresponds to the condition of  $0^\circ$  in Fig. 4.8 (b), and is again corrected into the condition  $90^\circ$ , i.e., vertical current injection, yielding  $195 \Omega$ .

It turned out that each of the tower had about the same impedance of  $200 \Omega$  as an independent tower, when it was simulated by direct method in the vertical arrangement.

Fisher *et al.* reported the surge impedance of a 345 kV double-circuit transmission tower to be  $135 \Omega$  [33] on the basis of the measurement in the vertical arrangement on a 25-to-1 reduced-scale model. The tower surge impedance of a typical double-circuit tower by direct method were characterized by the current splitting ratio at the top of the tower are estimated to be about  $205 \Omega$  for a vertical current injection and about  $135 \Omega$  for a horizontal one.

## 4.8 Computation Time

For the numerical analysis, the conductors of the system are divided into 10 m or 12 m segments. The internal impedance of the pulse generator is 5 k $\Omega$ . Computation is carried out in the frequency range of 39.06 kHz to 20 MHz with the incremental step of 39.06 MHz. This corresponds to the time range of 0 to 25.6  $\mu$ sec with 0.05  $\mu$ sec increments. The computation time with a Pentium II 300 MHz processor with 128 MB RAM is about 21 minutes for the maximum case.

## 4.9 Summary

The surge characteristics of an earth-wired tower struck by a lightning stroke are studied with the help of NEC-2. The type of the lightning current influences them, whether it is generated by a return stroke or by a downward travelling current or stroke to mid-span. The computed waveforms of the current splitting ratio into the tower and into one side of the earth wire shown in Figs. 4.5 (b), 4.6 (b) and 4.7. In Fig 4.6 (b) and 4.7, the injected current splits into the tower and earth wire at a fixed ratio until 0.8  $\mu$ sec, which is the arrival time of the reflected wave from the ground. In Fig. 4.5 (b), the current splitting into the tower increases gradually before 0.8  $\mu$ sec. This effect is ascribable to the induced current in the tower. The voltage in the upper insulator rises steeply and then saturates, while the rate of rise in others does less steeply. This is because the upper-phase conductor is more affected by induction from the earth wire whose voltage also rises exponentially.

These results can be used to estimate the tower surge impedance of the standard arrangement with a vertical current lead wire and a horizontal voltage measuring wire. The tower surge impedance representing the current splitting ratio at the tower top for a vertical stroke to the tower is higher than that characterized by the direct method for more than 25 %. On the other hand, the tower surge impedance representing the current splitting ratio for a stroke to mid-span or to an adjacent tower is about 10 % lower than that characterized by the direct method.



## Chapter 5

### Conclusions

Vertical conductor models with and without ground plane for the analysis of surge characteristics theoretically and numerically by NEC-2 were reported in this thesis. The applicability of NEC-2 to the electromagnetic field analysis of tower surge response is verified by comparing the computed results with theoretical results on simple structures such as reduced scale model of 60 cm, 90 cm and 120 cm. Simulation was also carried on four parallel conductors model and actual tower model by NEC-2. Although there are some restrictions in the structures that can be properly modeled for NEC-2, it is much more flexible than the classical modeling of a tower by a cylinder or a cone.

Simulation carried out reduced scale models, therefore, have hardly been employed in the practical calculation of the lightning performance of transmission lines but this approach is useful in understanding the lightning phenomena and the dynamic electromagnetic behavior of a three dimensional system struck by lightning particularly at the transient period.

The simulation results with NEC-2 are little bit far from the theoretical values, which may due to the effects of programming technique in NEC-2 to calculate currents in wire.

The propagation velocity of the electromagnetic wave inside the vertical conductor is found to be the same as the velocity of light.

On the basis of various simulating by NEC-2, the surge impedance of an independent double-circuit tower is estimated to be about 150  $\Omega$ ; when it is evaluated by the direct method, where a current lead wire simulating a lightning channel is stretched vertically and a voltage measuring wire is stretched horizontally. The tower surge impedance representing the current splitting ratio at the tower top for a vertical stroke to the tower is higher than that characterized by the indirect method for more than 25 %. On the other hand, the tower surge impedance representing the current splitting ratio for a stroke to mid-span or to an adjacent tower is about 10 % lower than that characterized by the direct method. The difference comes from different electromagnetic field around the tower influenced mainly by the electric fields associated with the fast-front currents propagating the tower, the earth wire and the current lead wire.

The surge characteristics of tower struck by a vertical lightning stroke are studied with the help of NEC-2. They are little influenced by the type of the lightning current, whether it is generated by a return stroke or it is generated by a downward traveling current wave.



The tower footing impedance evaluated from the reflected current exhibits initially a high value, which gradually falls off to the footing resistance. This apparent high footing impedance is physically ascribable to the distortion of the current wave propagating a tower. The distortion is partly caused by the strong axial electric field associated with the fast-front current wave itself, and is partly caused by the base-broadened structure towers, where a tower and its image behave as a non-homogeneous waveguide.

## Bibliography

- [1] "Lightning and Surge Protection", Report published by M.SYSTEM CO., LTD, Osaka 557-0063, Japan.
- [2] C. A. Jordan, "Lightning Computation For Transmission Line with Ground Wires," General Electric Review, vol. 34, pp.180-185, 1934.
- [3] R. Lundholm, R. B. Finn, Jr., and W. S. Price, "Calculation of Transmission Line Lightning Voltage by Field Concepts," AIEE Trans., pt. III, vol. 77, pp. 1271-1283, 1958.
- [4] C. F. Wagner and A. R. Hileman, "A New approach to calculation of lightning performance of transmission lines (part II, III)," AIEE Trans., pt. III, vol. 78/79, pp.996-1021/589-603, 1959/1960.
- [5] A. Sargent and M. Darveniza, "Tower surge impedance," IEEE Trans., vol. PAS-88, pp.680-687, 1969.
- [6] K. Okumura and A. Kijima, "A method for computing surge impedance of transmission line tower by electromagnetic field theory," IEE of Japan Trans. B, vol. 105, pp. 733-740, 1985.
- [7] M. Kawai, "Studies of the surge response on a transmission line tower," IEEE Trans., vol. PAS-83, pp. 30-34, 1964.
- [8] W. A. Chisholm, Y. L. Chow, and K. D. Srivastava, "Lightning surge response of transmission towers," IEEE Trans., vol. PAS-102, pp. 3232-3242, 1983.
- [9] W. A. Chisholm and Y. L. Chow, "Travel time of transmission tower," IEEE Trans., vol. PAS-104, pp. 2922-2928, 1985.
- [10] M. A. A. Wahab, I. Matsubara, and H. Kinoshita, "An experimental evaluation of some factors affecting tower surge impedance," Trans. IEE of Japan, vol. 107, pp.171-177, 1987.
- [11] T. Yamada, A. Mochizuki, J. Sawada, E. Zaima, T.Kawamura, A. Ametani, M. Ishii, and S. Kato, "Experimental evaluation of a LTHV tower model for lightning surge analysis," IEEE Trans., PWRD, vol. 10, pp. 393-402, 1995.
- [12] M. Ishii and Y. Baba, "Numerical electromagnetic field analysis of tower surge response," IEEE Trans., PWRD, vol. 12, pp. 483-488, 1997.

- [13] Y. Baba and M. Ishii, "Numerical electromagnetic field analysis on lightning surge response of tower with shield wire," *IEEE Trans. PWRD*, vol. 15, pp. 1010-1015, no. 3, Jul. 2000.
- [14] M. O. Goni, Masao Kodama, "The Finite Difference Time Domain Method for Sinusoidal Electromagnetic Fields", *ICICE Trans.* vol.e-85, no.3, March 2002.
- [15] R. F. Harrington, *Field computation by moment methods*, New York: Macmillan company, 1968.
- [16] K. S. Yee, "Numerical solution of initial boundary value problems involving Maxwell's equation in isotropic media," *IEEE Trans. Antennas Propagat.*, vol. AP-14, pp. 302-307, May 1996.
- [17] K. Tanabe, "Novel method for analyzing the transient behavior of grounding systems based on the FDTD method," in *Proc. IEEE Power Engineering Society winter meeting*, vol. 3, pp. 1128-1132, 2001.
- [18] G. J. Burke and A. J. Poggio, "Numerical Electromagnetic Code (NEC) - Method of Moments," *Naval Ocean Systems Center, Technical Document 116*, San Diego, Jan. 1980.
- [19] G. J. Burke, "Numerical electromagnetic code (NEC-4) -method of moments," *Lawrence Livermore National Laboratory, UCRL-MA-109338 pt. II*, Jan. 1992.
- [20] W. A. Chisholm and W. Janischewskyj, "Lightning surge response of ground electrodes," *IEEE Trans. Power Delivery*, vol.4, no.2, pp.1329-1337, Apr. 1989.
- [21] M. O. Goni, P. T Cheng, H. Takahashi, "Theoretical and Experimental Investigations of the Surge Response of a Vertical Conductor," in *Proc. IEEE Power Engineering Society*, vol. 2, pp. 699-704, 2002.
- [22] M. O. Goni and H. Takahashi, "Theoretical and experimental investigation of the surge response of a vertical conductor", *The ACES Journal*, vol.18, no.1, pp. 41-47, Mar. 2003.
- [23] M. O. Goni, E. Kaneko and H. Takahashi, "Thin wire representation of the vertical conductor surge simulation", *The ACES Journal*, vol.18, no.1, pp. 41-47, Mar. 2004.
- [24] H. Takahashi and M. Kodama, "Theoretical derivation of surge impedance about a vertical conductor." in *Proc. IEEE Power Engineering Society Int'l Conf.*, vol. 2, pp.688-693, 2002.
- [25] Md. Salah Uddin Yusuf, Md. Faruque Hossain, Md. Osman Goni, "Electromagnetic



- Simulation of Lightning Surge on Vertical Conductor Model”, Proc. of 3<sup>rd</sup> Int’l Conf. on Electrical and Computer Engg., ICECE, pp.163-167, 2004.
- [26] Md. Osman Goni, Md. Salah Uddin Yusuf, Md. Faruque Hossain, Md. Mostafizur Rahaman, E. Kaneko, H. Takahashi, “Theoretical Simulation and Experimental Investigation of the Surge Response of a Tower Model of Vertical Conductor”, Int’l journal of power and energy system, ACTA Press Paper (To be Published).
- [27] H. Takahashi, “New derivation method of the surge impedance on the tower model of a vertical conductor by electromagnetic field theory,” Trans. IEE Japan, vol.113-B, no.9, pp. 1028-1036, Sep.1993.
- [28] H. Takahashi, M. O. Goni, P.T Cheng, N. Arakawa, K. Matsuda, Y. Nakagawa, “Model Experiments and Simulation Analyses Concerning to the Lightning to the Communication Steel Tower and its Invasion to Control Building,” Bulletin, University of Ryukus, Sep.2001, Japan.
- [29] M. O. Goni, P.T Cheng, H.Takahashi, “Investigation of Surge Response of a Vertical Conductor,” National Conference of Plasma Science, PST-02-17, IEE of Japan, March 8, 2002, Japan.
- [30] H. Takahashi, “A consideration on the vertical conductor problem,” Proc. of ICEE, pp. 635-638, 2001.
- [31] Y. Baba and M. Ishii, “Numerical electromagnetic field analysis on measuring method of tower surge response,” IEEE Trans. PWRD, vol.14, pp.630-635, no.2 Apr. 1999.
- [32] A. Asakawa, K. Miyake, S. Yokoyama, T. Shindo, T.Yokota and T. Sakai, “Two Types of Lightning Discharges to a High Stack on the Coast of the Sea of Japan in Winter”, IEEE Trans. Power Delivery, vol.2, no.3, pp. 1222-1231, Jul. 1997.
- [33] F. A. Fisher, J. G. Anderson and J. H. Hagenguth, “Determination of lightning response of transmission lines by means of geometric models.” AIEE Trans. pt. III, vol. 78, pp. 1725-1736, Feb.1960.
- [34] M. Ishii, “Experimental study for insulation design of overhead transmission lines,” Ph.D thesis, The University of Tokyo, Dec.1975.
- [35] “RCS computer program BRACKT, log-periodic scattering array program II,” MBAssociates Report, no. MB-R-69/46, Contact no. F04801-68-C-0188, 1969.
- [36] “Antenna modeling program,” MBAssociates report, no. MB-R-74/46, 74/62, 1974.



## **Appendix A**

### **History and Availability of NEC-MoM Codes**

The first in a series of NEC-MoM codes was BRACK [35] developed at MBAssociates in San Ramon, California. BRACK solved Pocklington's integral equation for thin wires with a three-term sinusoidal current expansion and point matching of the boundary condition. This code could model wire antennas including the effect of interaction with a finitely conducting ground through the Fresnel reflection-coefficient approximation. However, BRACK was used mainly by its developers.

The Antenna Modeling Program (AMP) [36] was the first code released for use by public users. AMP also solved Pocklington's integral equation for thin wires with a three term sinusoidal current expansion and point matching. The current expansion was chosen so that the current on a segment, with the form  $A_i + B_i \sin ks + C_i \cos ks$ , when extrapolated to the centers of the adjacent segments would coincide with the values of current on those segments. At a junction of several wires, the current was extrapolated to the center of a "phantom segment" whose length was the average of the connected segments. This extrapolation procedure smoothed the current distribution along wires, but still left discontinuities in current and charge density. AMP included options to model lumped or distributed loading on wires, transmission lines and networks.

AMP-2 included a magnetic field integral equation model for surfaces while the previous version was restricted to modeling thin wires.

NEC-1 was developed from AMP-2. It included a new way of implementing the three-term sinusoidal current expansion so that current and charge density exactly satisfied continuity conditions imposed at the junctions. The current was forced to satisfy Kirchhoff's current law at the junction, and the charge densities on wires were related to a function of the log of wire radius to provide approximate continuity of potential.

NEC-2 added a solution for wires over a lossy ground by implementing the rigorous Sommerfeld-integral approach.

NEC-3 [18] extended the Sommerfeld-Integral ground model to wires buried in the ground or penetrating from air into ground.

NEC-4 [19] retains all of the capabilities of NEC-3, with changes and additions to improve the accuracy for stepped-radius wires and electrically small segments, and to add end caps and insulated wires.

The author employs NEC-2 in the present study, since later versions, NEC-3 and NEC-4, are available only to the citizens of the United States and Canada, or to the users who are licensed from Lawrence Livermore National Laboratory.



The documentation for NEC-2 is officially available from the National Technical Information Service, U.S. Department of Commerce.

National Technical Information Service

U.S. Department of Commerce

Springfield, Virginia 22161

Phone: + 1- 703- 487- 4650

It consists of three volumes; the theory, the source code in Fortran and the user's guide. The current price is about 200 dollars.

The volumes of the theory and the user's guide are also obtained on a WWW site at

<http://members.home.net/nec2/>

The information's on the free executables of NEC-2 and commercial programs sold by vendors are also available on the above site.

Recent materials on the MoM theory and its applications contain detailed descriptions of the MoM, and they are useful for persons who wish to learn to use NEC-MoM codes.

## **Appendix B**

### **Sample Input Data to NEC-2 for Single Vertical Conductor**

CM SINGLE VERTICAL CONDUCTOR FOR VOLTAGE

CM Horizontally applied source at the top (Horizontal Input Fig. 2.3)

CM N = 512, DT = 0.25E-09, SEC DL = 10 cm, r = 0.0005 m only vertical conductor

CE PERFECTLY CONDUCTING GROUND

GW	1	6	0.0	0.0	0.6	0.0	0.0	0.0	0.0005
GW	2	30	0.0	3.0	0.6	0.0	0.0	0.6	0.0005
GW	3	6	0.0	3.0	0.6	0.0	3.0	0.0	0.0005
GW	4	20	0.0	0.0	0.6	2.0	0.0	0.6	0.0005
GW	5	6	2.0	0.0	0.6	2.0	0.0	0.0	0.0005
GE	1								
GN	1								
LD	4	2	1	5.1E+02					
LD	4	5	6	0.1					
LD	4	1	6	0.1					
LD	4	4	1	1.0E+04					
FR	0	257		7.813	7.813				
EX	0	2	1	00	5.0E+0	0.0			
PT	0	2	1						
XQ									
EN									

CM SINGLE VERTICAL CONDUCTOR FOR CURRENT

CM Horizontally applied source at the top (Horizontal Input Fig. 2.3)

CM N = 512, DT = 0.25E-09, SEC DL = 10 cm, r = 0.0005 m

CE PERFECTLY CONDUCTING GROUND

GW	1	6	0.0	0.0	0.6	0.0	0.0	0.0	0.0005
GW	2	30	0.0	3.0	0.6	0.0	0.0	0.6	0.0005
GW	3	6	0.0	3.0	0.6	0.0	3.0	0.0	0.0005
GW	4	20	0.0	0.0	0.6	2.0	0.0	0.6	0.0005
GW	5	6	2.0	0.0	0.6	2.0	0.0	0.0	0.0005
GE	1								
GN	1								
LD	4	2	1	5.1E+02					
LD	4	5	6	0.1					
LD	4	1	6	0.1					
LD	4	4	1	1.0E+04					
FR	0	257		7.813	7.813				
EX	0	2	1	00	5.0E+0	0.0			
PT	0	1	1						
XQ									
EN									



CM SINGLE VERTICAL CONDUCTOR FOR VOLTAGE

CM Vertically applied source (Vertical input Fig. 2.4)

CM N=512, DT= 0.25E-09 SEC, DL=10 cm, r=.0005 m only vertical conductor

CE PERFECTLY CONDUCTING GROUND

GW	1	6	0.0	0.0	0.6	0.0	0.0	0.0	0.0005
GW	2	20	0.0	0.0	0.6	2.0	0.0	0.6	0.0005
GW	3	6	2.0	0.0	0.6	2.0	0.0	0.0	0.0005
GW	4	20	0.0	0.0	2.6	0.0	0.0	0.6	0.0005
GE	1								
GN	1								
LD	4	4	20		5.1E+02				
LD	4	1	1		0.1				
LD	4	3	6		0.1				
LD	4	2	1		1.0E+04				
FR	0	257			7.8125	7.8125			
EX	0	4	20	00	5.0E+0	0.0			
PT	0	2	1						
XQ									
EN									

CM SINGLE VERTICAL CONDUCTOR FOR CURRENT

CM Vertically applied source (Vertical input Fig. 2.4)

CM N=512, DT=0.25E-09 SEC, DL=10 cm, r=.0005m only vertical conductor

CE PERFECTLY CONDUCTING GROUND

GW	1	6	0.0	0.0	0.6	0.0	0.0	0.0	0.0005
GW	2	20	0.0	0.0	0.6	2.0	0.0	0.6	0.0005
GW	3	6	2.0	0.0	0.6	2.0	0.0	0.0	0.0005
GW	4	20	0.0	0.0	2.6	0.0	0.0	0.6	0.0005
GE	1								
GN	1								
LD	4	4	20		5.1E+02				
LD	4	1	1		0.1				
LD	4	3	6		0.1				
LD	4	2	1		1.0E+04				
FR	0	257			7.8125	7.8125			
EX	0	4	20	00	5.0E+0	0.0			
PT	0	1	1						
XQ									
EN									

## **Appendix C**

### **Sample Input Data to NEC-2 for Four Parallel Vertical Conductors**

```

CM FOUR VERTICAL PARALLEL CONDUCTORS FOR VOLTAGE
CM Horizontally applied source at the top (Horizontal Input for Fig.3.3)
CM N=512 DT=1.25E-09 SEC
CE PERFECTLY CONDUCTING GROUND
GW 1 10 0.0 0.0 3.0 0.0 0.0 0.0 0.0165
GW 2 10 0.0 0.404 3.0 0.0 0.404 0.0 0.0165
GW 3 10 0.404 0.404 3.0 0.404 0.404 0.0 0.0165
GW 4 10 0.404 0.0 3.0 0.404 0.0 0.0 0.0165
GW 5 2 0.0 0.0 3.0 0.0 0.404 3.0 0.0165
GW 6 2 0.0 0.404 3.0 0.404 0.404 3.0 0.0165
GW 7 2 0.404 0.404 3.0 0.404 0.0 3.0 0.0165
GW 8 2 0.404 0.0 3.0 0.0 0.0 3.0 0.0165
GW 9 30 0.202 9.404 3.0 0.202 0.404 3.0 0.0165
GW 10 10 0.202 9.404 3.0 0.202 9.404 0.0 0.0165
GW 11 30 0.404 0.0 3.0 9.404 0.0 3.0 0.0165
GW 12 10 9.404 0.0 3.0 9.404 0.0 0.0 0.0165
GE 1
GN 1
LD 4 9 20 20 5.0E+03
LD 4 10 10 10 467.0
LD 4 12 10 10 467.0
LD 4 11 1 1 1.0E+04
FR 0 257 1.5625 1.5625
EX 0 9 20 00 5.0E+03 0.0
PT 0 11 1
XQ
EN

```

```

CM FOUR VERTICAL PARALLEL CONDUCTORS FOR CURRENT
CM Horizontally applied source at the top (Horizontal Input for Fig.3.3)
CM N=512 DT=1.25E-09 SEC
CE PERFECTLY CONDUCTING GROUND
GW 1 10 0.0 0.0 3.0 0.0 0.0 0.0 0.0165
GW 2 10 0.0 0.404 3.0 0.0 0.404 0.0 0.0165
GW 3 10 0.404 0.404 3.0 0.404 0.404 0.0 0.0165
GW 4 10 0.404 0.0 3.0 0.404 0.0 0.0 0.0165
GW 5 2 0.0 0.0 3.0 0.0 0.404 3.0 0.0165
GW 6 2 0.0 0.404 3.0 0.404 0.404 3.0 0.0165
GW 7 2 0.404 0.404 3.0 0.404 0.0 3.0 0.0165
GW 8 2 0.404 0.0 3.0 0.0 0.0 3.0 0.0165
GW 9 30 0.202 9.404 3.0 0.202 0.404 3.0 0.0165
GW 10 10 0.202 9.404 3.0 0.202 9.404 0.0 0.0165
GW 11 30 0.404 0.0 3.0 9.404 0.0 3.0 0.0165
GW 12 10 9.404 0.0 3.0 9.404 0.0 0.0 0.0165
GE 1
GN 1
LD 4 9 20 20 5.0E+03
LD 4 10 10 10 467.0
LD 4 12 10 10 467.0
LD 4 11 1 1 1.0E+04
FR 0 257 1.5625 1.5625
EX 0 9 20 00 5.0E+03 0.0
PT 0 9 30
XQ
EN

```



CM FOUR PARALLEL VERTICAL CONDUCTOR FOR VOLTAGE

CM Vertically applied source for cross configuration of Fig.3.6(a)

CM N=512 DT= 1.25E-09 SEC

CE PERFECTLY CONDUCTING GROUND

CM N=512 DT= 1.25E-09 SEC

CE PERFECTLY CONDUCTING GROUND

GW	1	10	0.0	0.0	3.0	0.0	0.0	0.0	0.0165
GW	2	10	0.0	0.404	3.0	0.0	0.404	0.0	0.0165
GW	3	10	0.404	0.404	3.0	0.404	0.404	0.0	0.0165
GW	4	10	0.404	0.0	3.0	0.404	0.0	0.0	0.0165
GW	5	2	0.0	0.0	3.0	0.0	0.404	3.0	0.0165
GW	6	2	0.0	0.404	3.0	0.404	0.404	3.0	0.0165
GW	7	2	0.404	0.404	3.0	0.404	0.0	3.0	0.0165
GW	8	2	0.404	0.0	3.0	0.0	0.0	3.0	0.0165
GW	9	30	0.202	0.202	12.0	0.202	0.202	3.0	0.0165
GW	10	30	0.404	0.0	3.0	9.404	0.0	3.0	0.0165
GW	11	10	9.404	0.0	3.0	9.404	0.0	0.0	0.0165
GW	12	2	0.0	0.0	3.0	0.402	0.404	3.0	0.0165
GW	13	2	0.0	0.402	3.0	0.404	0.0	3.0	0.0165
GE	1								
GN	1								
LD	4	9	30	30	5.0E+03				
LD	4	11	10	10	467.0				
LD	4	10	1	1	1.0E+04				
FR	0	257	0	0	1.5625	1.5625			
EX	0	9	30	00	5.0E+3	0.0			
PT	0	11	1						
XQ									
EN									

CM FOUR PARALLEL VERTICAL CONDUCTOR FOR CURRENT

CM Vertically applied source for cross configuration of Fig.3.6(a)

CM N=512 DT= 1.25E-09 SEC

CE PERFECTLY CONDUCTING GROUND

CM N=512 DT= 1.25E-09 SEC

CE PERFECTLY CONDUCTING GROUND

GW	1	10	0.0	0.0	3.0	0.0	0.0	0.0	0.0165
GW	2	10	0.0	0.404	3.0	0.0	0.404	0.0	0.0165
GW	3	10	0.404	0.404	3.0	0.404	0.404	0.0	0.0165
GW	4	10	0.404	0.0	3.0	0.404	0.0	0.0	0.0165
GW	5	2	0.0	0.0	3.0	0.0	0.404	3.0	0.0165
GW	6	2	0.0	0.404	3.0	0.404	0.404	3.0	0.0165
GW	7	2	0.404	0.404	3.0	0.404	0.0	3.0	0.0165
GW	8	2	0.404	0.0	3.0	0.0	0.0	3.0	0.0165
GW	9	30	0.202	0.202	12.0	0.202	0.202	3.0	0.0165
GW	10	30	0.404	0.0	3.0	9.404	0.0	3.0	0.0165
GW	11	10	9.404	0.0	3.0	9.404	0.0	0.0	0.0165
GW	12	2	0.0	0.0	3.0	0.402	0.404	3.0	0.0165
GW	13	2	0.0	0.402	3.0	0.404	0.0	3.0	0.0165
GE	1								
GN	1								
LD	4	9	30	30	5.0E+03				
LD	4	11	10	10	467.0				
LD	4	10	1	1	1.0E+04				
FR	0	257	0	0	1.5625	1.5625			
EX	0	9	30	00	5.0E+3	0.0			
PT	0	9	30						
XQ									
EN									

CM FOUR PARALLEL VERTICAL CONDUCTOR FOR VOLTAGE

CM Vertically applied source for cross configuration of Fig.3.6(b)

CM N=512 DT= 1.25E-09 SEC

CE PERFECTLY CONDUCTING GROUND

GW	1	10	0.0	0.0	3.0	0.0	0.0	0.0	0.0165
GW	2	10	0.0	0.404	3.0	0.0	0.404	0.0	0.0165
GW	3	10	0.404	0.404	3.0	0.404	0.404	0.0	0.0165
GW	4	10	0.404	0.0	3.0	0.404	0.0	0.0	0.0165
GW	5	2	0.0	0.0	3.0	0.0	0.404	3.0	0.0165
GW	6	2	0.0	0.404	3.0	0.404	0.404	3.0	0.0165
GW	7	2	0.404	0.404	3.0	0.404	0.0	3.0	0.0165
GW	8	2	0.404	0.0	3.0	0.0	0.0	3.0	0.0165
GW	9	30	0.404	0.0	12.0	0.404	0.0	3.0	0.0165
GW	10	30	0.404	0.0	3.0	9.404	0.0	3.0	0.0165
GW	11	10	9.404	0.0	3.0	9.404	0.0	0.0	0.0165
GE	1								
GN	1								
LD	4	9	30	30	5.0E+03				
LD	4	11	10	10	467.0				
LD	4	10	1	1	1.0E+04				
FR	0	257	0	0	1.5625	1.5625			
EX	0	9	30	00	5.0E+3	0.0			
PT	0	10	1						
XQ									

CM FOUR PARALLEL VERTICAL CONDUCTOR FOR CURRENT

CM Vertically applied source for cross configuration of Fig.3.6(b)

CM N=512 DT= 1.25E-09 SEC

CE PERFECTLY CONDUCTING GROUND

GW	1	10	0.0	0.0	3.0	0.0	0.0	0.0	0.0165
GW	2	10	0.0	0.404	3.0	0.0	0.404	0.0	0.0165
GW	3	10	0.404	0.404	3.0	0.404	0.404	0.0	0.0165
GW	4	10	0.404	0.0	3.0	0.404	0.0	0.0	0.0165
GW	5	2	0.0	0.0	3.0	0.0	0.404	3.0	0.0165
GW	6	2	0.0	0.404	3.0	0.404	0.404	3.0	0.0165
GW	7	2	0.404	0.404	3.0	0.404	0.0	3.0	0.0165
GW	8	2	0.404	0.0	3.0	0.0	0.0	3.0	0.0165
GW	9	30	0.404	0.0	12.0	0.404	0.0	3.0	0.0165
GW	10	30	0.404	0.0	3.0	9.404	0.0	3.0	0.0165
GW	11	10	9.404	0.0	3.0	9.404	0.0	0.0	0.0165
GE	1								
GN	1								
LD	4	9	30	30	5.0E+03				
LD	4	11	10	10	467.0				
LD	4	10	1	1	1.0E+04				
FR	0	257	0	0	1.5625	1.5625			
EX	0	9	30	00	5.0E+3	0.0			
PT	0	9	30						
XQ									
EN									

CM FOUR PARALLEL VERTICAL CONDUCTOR FOR VOLTAGE

CM Vertically applied source for plus configuration of Fig.3.6(c)

CM N=512 DT= 1.25E-09 SEC

CE PERFECTLY CONDUCTING GROUND

GW 1	10	0.0	0.0	3.0	0.0	0.0	0.0	0.0165
GW 2	10	0.0	0.404	3.0	0.0	0.404	0.0	0.0165
GW 3	10	0.404	0.404	3.0	0.404	0.404	0.0	0.0165
GW 4	10	0.404	0.0	3.0	0.404	0.0	0.0	0.0165
GW 5	2	0.0	0.0	3.0	0.0	0.404	3.0	0.0165
GW 6	2	0.0	0.404	3.0	0.404	0.404	3.0	0.0165
GW 7	2	0.404	0.404	3.0	0.404	0.0	3.0	0.0165
GW 8	2	0.404	0.0	3.0	0.0	0.0	3.0	0.0165
GW 9	30	0.202	0.202	12.0	0.202	0.202	3.0	0.0165
GW 10	30	0.404	0.0	3.0	9.404	0.0	3.0	0.0165
GW 11	10	9.404	0.0	3.0	9.404	0.0	0.0	0.0165
GW 12	2	0.202	0.0	3.0	0.202	0.404	3.0	0.0165
GW 13	2	0.0	0.202	3.0	0.404	0.202	3.0	0.0165
GE 1								
GN 1								
LD 4	9	30	30	5.0E+03				
LD 4	11	10	10	467.0				
LD 4	10	1	1	1.0E+04				
FR 0	257	0	0	1.5625	1.5625			
EX 0	9	30	00	5.0E+3	0.0			
PT 0	10	1						
XQ								
EN								

CM FOUR PARALLEL VERTICAL CONDUCTOR FOR CURRENT

CM Vertically applied source for plus configuration of Fig.3.6(c)

CM N=512 DT= 1.25E-09 SEC

CE PERFECTLY CONDUCTING GROUND

GW 1	10	0.0	0.0	3.0	0.0	0.0	0.0	0.0165
GW 2	10	0.0	0.404	3.0	0.0	0.404	0.0	0.0165
GW 3	10	0.404	0.404	3.0	0.404	0.404	0.0	0.0165
GW 4	10	0.404	0.0	3.0	0.404	0.0	0.0	0.0165
GW 5	2	0.0	0.0	3.0	0.0	0.404	3.0	0.0165
GW 6	2	0.0	0.404	3.0	0.404	0.404	3.0	0.0165
GW 7	2	0.404	0.404	3.0	0.404	0.0	3.0	0.0165
GW 8	2	0.404	0.0	3.0	0.0	0.0	3.0	0.0165
GW 9	30	0.202	0.202	12.0	0.202	0.202	3.0	0.0165
GW 10	30	0.404	0.0	3.0	9.404	0.0	3.0	0.0165
GW 11	10	9.404	0.0	3.0	9.404	0.0	0.0	0.0165
GW 12	2	0.202	0.0	3.0	0.202	0.404	3.0	0.0165
GW 13	2	0.0	0.202	3.0	0.404	0.202	3.0	0.0165
GE 1								
GN 1								
LD 4	9	30	30	5.0E+03				
LD 4	11	10	10	467.0				
LD 4	10	1	1	1.0E+04				
FR 0	257	0	0	1.5625	1.5625			
EX 0	9	30	00	5.0E+3	0.0			
PT 0	9	30						
XQ								
EN								



## **Appendix D**

### **Sample Input Data to NEC-2 for Actual Tower**

```

CM ACTUAL TOWER MODEL
CM Vertically applied source
CM N=512 DT= 50E-09 SEC
CE PERFECTLY CONDUCTING GROUND
GW 1 1 -5.0 -5.0 120.0 -5.0 -5.0 108.0 0.1
GW 2 1 5.0 -5.0 120.0 5.0 -5.0 108.0 0.1
GW 3 1 5.0 5.0 120.0 5.0 5.0 108.0 0.1
GW 4 1 -5.0 5.0 120.0 -5.0 5.0 108.0 0.1
GW 5 2 -5.0 -5.0 108.0 -5.0 -5.0 84.0 0.15
GW 6 2 5.0 -5.0 108.0 5.0 -5.0 84.0 0.15
GW 7 2 5.0 5.0 108.0 5.0 5.0 84.0 0.15
GW 8 2 -5.0 5.0 108.0 -5.0 5.0 84.0 0.15
GW 9 1 -5.0 -5.0 84.0 -5.0 -5.0 72.0 0.2
GW 10 1 5.0 -5.0 84.0 5.0 -5.0 72.0 0.2
GW 11 1 5.0 5.0 84.0 5.0 5.0 72.0 0.2
GW 12 1 -5.0 5.0 84.0 -5.0 5.0 72.0 0.2
GW 13 1 -5.0 -5.0 72.0 -5.0 -5.0 60.0 0.25
GW 14 1 5.0 -5.0 72.0 5.0 -5.0 60.0 0.25
GW 15 1 5.0 5.0 72.0 5.0 5.0 60.0 0.25
GW 16 1 -5.0 5.0 72.0 -5.0 5.0 60.0 0.25
GW 17 1 -5.0 -5.0 60.0 -6.2 -6.2 48.0 0.25
GW 18 1 5.0 -5.0 60.0 6.2 -6.2 48.0 .25
GW 19 1 5.0 5.0 60.0 6.2 6.2 48.0 0.25
GW 20 1 -5.0 5.0 60.0 -6.2 6.2 48.0 0.25
GW 21 2 -6.2 -6.2 48.0 -8.6 -8.6 24.0 0.3
GW 22 2 6.2 -6.2 48.0 8.6 -8.6 24.0 0.3
GW 23 2 6.2 6.2 48.0 8.6 8.6 24.0 0.3
GW 24 2 -6.2 6.2 48.0 -8.6 8.6 24.0 0.3
GW 25 2 -8.6 -8.6 24.0 -11.0 -11.0 0.0 0.35
GW 26 2 8.6 -8.6 24.0 11.0 -11.0 0.0 0.35
GW 27 2 8.6 8.6 24.0 11.0 11.0 0.0 0.35
GW 28 2 -8.6 8.6 24.0 -11.0 11.0 0.0 0.35
GW 29 1 -5.0 -5.0 120.0 5.0 -5.0 120.0 0.1
GW 30 1 5.0 -5.0 120.0 5.0 5.0 120.0 0.1
GW 31 1 5.0 5.0 120.0 -5.0 5.0 120.0 0.1
GW 32 1 -5.0 5.0 120.0 -5.0 -5.0 120.0 0.1
GW 33 40 5.0 -5.0 600.0 5.0 -5.0 120.0 0.1
GW 34 40 -15.0 -5.0 108.0 -15.0 -485.0 108.0 0.1
GW 35 9 -15.0 -485.0 108.0 -15.0 -485.0 0.0 0.1
GW 36 40 -15.0 -5.0 108.0 -15.0 475.0 108.0 0.1
GW 37 9 -15.0 475.0 108.0 -15.0 475.0 0.0 0.1
GW 38 1 -5.0 -5.0 108.0 -15.0 -5.0 108.0 0.1
GW 39 40 -5.0 -5.0 120.0 -5.0 -485.0 120.0 0.1
GW 40 10 -5.0 -485.0 120.0 -5.0 -485.0 0.0 0.1
GW 41 40 -5.0 5.0 120.0 -5.0 485.0 120.0 0.1
GW 42 10 -5.0 485.0 120.0 -5.0 485.0 0.0 0.1
GE 1
GN 1
LD 4 33 40 40 5.0E+03
LD 4 35 9 9 461.0
LD 4 37 9 9 461.0
LD 4 40 10 10 467.0
LD 4 42 10 10 467.0
LD 4 38 1 1 1.0E+05
LD 4 25 2 2 40.0
LD 4 26 2 2 40.0
LD 4 27 2 2 40.0
LD 4 28 2 2 40.0
FR 0 257 0 0 3.906E-2 3.906E-02
EX 0 33 40 00 5.0E+3 0.0
PT 0 38 1
XQ
EN

```

CM ACTUAL TOWER MODEL

CM Horizontally applied source

CM N=512 DT= 50E-09 SEC

CE PERFECTLY CONDUCTING GROUND

GW	1	1	-5.0	-5.0	120.0	-5.0	-5.0	108.0	0.1
GW	2	1	5.0	-5.0	120.0	5.0	-5.0	108.0	0.1
GW	3	1	5.0	5.0	120.0	5.0	5.0	108.0	0.1
GW	4	1	-5.0	5.0	120.0	-5.0	5.0	108.0	0.1
GW	5	2	-5.0	-5.0	108.0	-5.0	-5.0	84.0	0.15
GW	6	2	5.0	-5.0	108.0	5.0	-5.0	84.0	0.15
GW	7	2	5.0	5.0	108.0	5.0	5.0	84.0	0.15
GW	8	2	-5.0	5.0	108.0	-5.0	5.0	84.0	0.15
GW	9	1	-5.0	-5.0	84.0	-5.0	-5.0	72.0	0.2
GW	10	1	5.0	-5.0	84.0	5.0	-5.0	72.0	0.2
GW	11	1	5.0	5.0	84.0	5.0	5.0	72.0	0.2
GW	12	1	-5.0	5.0	84.0	-5.0	5.0	72.0	0.2
GW	13	1	-5.0	-5.0	72.0	-5.0	-5.0	60.0	0.25
GW	14	1	5.0	-5.0	72.0	5.0	-5.0	60.0	0.25
GW	15	1	5.0	5.0	72.0	5.0	5.0	60.0	0.25
GW	16	1	-5.0	5.0	72.0	-5.0	5.0	60.0	0.25
GW	17	1	-5.0	-5.0	60.0	-6.2	-6.2	48.0	0.25
GW	18	1	5.0	-5.0	60.0	6.2	-6.2	48.0	0.25
GW	19	1	5.0	5.0	60.0	6.2	6.2	48.0	0.25
GW	20	1	-5.0	5.0	60.0	-6.2	6.2	48.0	0.25
GW	21	2	-6.2	-6.2	48.0	-8.6	-8.6	24.0	0.3
GW	22	2	6.2	-6.2	48.0	8.6	-8.6	24.0	0.3
GW	23	2	6.2	6.2	48.0	8.6	8.6	24.0	0.3
GW	24	2	-6.2	6.2	48.0	-8.6	8.6	24.0	0.3
GW	25	2	-8.6	-8.6	24.0	-11.0	-11.0	0.0	0.35
GW	26	2	8.6	-8.6	24.0	11.0	-11.0	0.0	0.35
GW	27	2	8.6	8.6	24.0	11.0	11.0	0.0	0.35
GW	28	2	-8.6	8.6	24.0	-11.0	11.0	0.0	0.35
GW	29	1	-5.0	-5.0	120.0	5.0	-5.0	120.0	0.1
GW	30	1	5.0	-5.0	120.0	5.0	5.0	120.0	0.1
GW	31	1	5.0	5.0	120.0	-5.0	5.0	120.0	0.1
GW	32	1	-5.0	5.0	120.0	-5.0	-5.0	120.0	0.1
GW	33	40	605.0	-5.0	120.0	5.0	-5.0	120.0	0.1
GW	34	40	-15.0	-5.0	108.0	-15.0	-485.0	108.0	0.1
GW	35	9	-15.0	-485.0	108.0	-15.0	-485.0	0.0	0.1
GW	36	40	-15.0	-5.0	108.0	-15.0	475.0	108.0	0.1
GW	37	9	-15.0	475.0	108.0	-15.0	475.0	0.0	0.1
GW	38	1	-5.0	-5.0	108.0	-15.0	-5.0	108.0	0.1
GW	39	40	-5.0	-5.0	120.0	-5.0	-485.0	120.0	0.1
GW	40	10	-5.0	-485.0	120.0	-5.0	-485.0	0.0	0.1
GW	41	40	-5.0	5.0	120.0	-5.0	485.0	120.0	0.1
GW	42	10	-5.0	485.0	120.0	-5.0	485.0	0.0	0.1
GW	43	10	605.0	-5.0	120.0	605.0	0.0	0.0	0.1
GE	1								
GN	1								
LD	4	33	20	20	5.0E+03				
LD	4	35	9	9	461.0				
LD	4	40	10	10	467.0				
LD	4	42	10	10	467.0				
LD	4	38	1	1	1.0E+05				
LD	4	25	2	2	40.0				
LD	4	26	2	2	40.0				
LD	4	27	2	2	40.0				
LD	4	28	2	2	40.0				
FR	0	257	0	0	3.906E-2	3.906E-02			
EX	0	33	20	00	5.0E+3	0.0			
PT	0	38	1						
XQ									
EN									